Modeling photosynthesis of discontinuous plant canopies by linking Geometric Optical Radiative Transfer model with biochemical processes

Qinchuan Xin [1*], Peng Gong [1, 2, 3, *], Wenyu Li [1]

[1] Ministry of Education Key Laboratory for Earth System Modeling, Tsinghua University, Beijing, China

[2] Joint Center for Global Change Studies, Beijing, China

[3] Environmental Science, Policy and Management and Geography, University of California, Berkeley, CA, USA

[*] Correspondence to: xqcchina@gmail.com (Qinchuan Xin)

penggong@tsinghua.edu.cn (Peng Gong)

Mailing Address:
Tsinghua University
Mengminwei South Building Room 920
Beijing 100084, China

Abstract

Modeling vegetation photosynthesis is essential for understanding carbon exchanges between terrestrial ecosystems and the atmosphere. The radiative transfer process within plant canopies is one of the key drivers that regulate canopy photosynthesis. Most vegetation cover consists of discrete plant crowns, of which the physical observation departs from the underlying assumption of a homogenous and uniform medium in classic radiative transfer theory. Here we advance the Geometric Optical Radiative Transfer (GORT) model to simulate photosynthesis activities for discontinuous plant canopies. We separate radiation absorption into two components that are absorbed by sunlit and shaded leaves, and derive analytical solutions by integrating over the canopy layer. To model leaf-level and canopy-level photosynthesis, leaf light absorption is then linked to the biochemical process of gas diffusion through leaf stomata. The canopy gap probability derived from GORT differs from classic radiative transfer theory, especially when the leaf area index is high, due to leaf clumping effects. Tree characteristics such as tree density, crown shape, and canopy length affect leaf clumping and regulate radiation interception. Modeled gross primary production (GPP) for two deciduous forest stands could explain more than 80% of the variance of flux tower measurements at both near hourly and daily time scales. We demonstrate that ambient CO_2 concentrations influence daytime vegetation photosynthesis, which needs to be considered in biogeochemical models. The proposed model is complementary to classic radiative transfer theory and shows promise in modeling the radiative transfer process and photosynthetic activities over discontinuous forest canopies.

Key words: gross primary production; flux tower; carbon cycle; radiative transfer; carbon assimilation

1. Introduction

Terrestrial plants assimilate atmospheric carbon dioxide through photosynthesis (Keenan et al., 2013; Myneni et al., 1997). The climate system, in turn, affects vegetation development and photosynthetic activities (Broich et al., 2014; Xia et al., 2014; Yi et al., 2010). Photosynthesis, accompanied by exchanges of heat, water vapor, and trace gases within the planetary boundary layer, modifies microclimates and local environments and determines ecosystem functions and services (Peng et al., 2014; Xu et al., 2013). The complex biosphere/atmosphere feedbacks are dynamic and interactive (Bonan, 2008; Heimann and Reichstein, 2008), such that robust numerical models that simulate vegetation photosynthesis are required in terrestrial ecosystem models to understand the global carbon cycle (Cramer et al., 2001; Kucharik et al., 2006).

Vegetation photosynthesis activity is regulated by environmental factors, and the light environment within plant canopies is one of the key drivers (Law et al., 2002; Pearcy and Sims, 1994). Biophysical models such as Production Efficiency Models assume linear relationships between absorbed photosynthetically active radiation (APAR) and vegetation primary production (Field et al., 1995; Monteith, 1977; Potter et al., 1993; Prince and Goward, 1995; Running et al., 2000). Because vegetation photosynthesis harvests solar radiation by green chlorophyll, recent studies have attempted to quantify the fractions of APAR that are absorbed by green chlorophyll (Zhang et al., 2014; Zhang et al., 2005). Physiologically, plants assimilate carbon dioxide via the biochemical diffusion processes through stomata, numerous small pores on the leaf surfaces (Collatz et al., 1991; Farquhar and Sharkey, 1982). Stomata can open and close in response to microenvironments, thereby regulating plant carbon uptake (Bonan, 2002). Field physiological studies have accumulated detailed information on the behavior of stomata under certain environmental conditions (Schulze et al., 1994), in which sunlight irradiance plays a vital role (Ball et al., 1987). In this domain, linking the physical process of radiative transfer within plant canopies with the biochemical process of gas diffusion through leaf stomata is essential for accurate representation of vegetation photosynthesis.

63

Radiative transfer within a plant canopy is determined by many factors such as the partition of incoming solar radiation, solar illumination geometry, terrain slope and aspects, canopy structure, leaf angle distribution, and leaf and substrate spectral properties (Baldocchi et al., 1985; Fan et al., 2014; Schaaf et al., 1994). Classic radiative transfer theory assumes that plant leaves are randomly distributed in three-dimensional space within a homogeneous canopy layer (Goudriaan, 1977; Myneni et al., 1990). The canopy radiative transfer process can be simply characterized by leaf area index (LAI) and leaf angle distribution (LAD). Three-dimensional, multi-layer, and two-leaf radiative transfer models have been developed to simulate leaf absorption of solar irradiance and canopy photosynthesis (Myneni, 1991; Pury and Farquhar, 1997; Ryu et al., 2011; Sellers, 1985). Although classic radiative transfer theory holds well for dense vegetation canopies, most vegetation canopies, especially arboreal canopies, consist of discrete crowns in reality (Yuan et al., 2013). Leaves are clumped within individual crowns, such that more sunlight penetrates to understory layers and the ground surfaces (He et al., 2012; Ni-Meister et al., 2010). Tree crowns also cast shadows on one another and on the background, resulting in self-shadowing effects as described by the geometric-optical theory (Li and Strahler, 1992). Given natural differences in the radiative transfer process between homogenous and discontinuous plant canopies, it is important to understand and account for the influence of crown shape and tree structure on canopy radiation absorption and vegetation photosynthesis.

80

To address the radiative transfer process in discontinuous canopies, the Geometric-Optical Radiative-Transfer (GORT) model conceptually combines geometric optical principles for canopy structure and radiative transfer theory for volumetric scattering within canopy crowns (Li et al., 1995). The geometric optical method is used to characterize the process by which sunlight passes directly to the ground surface without reaching any canopy crowns. The radiative transfer principle is applied to model the probability of light penetration as it travels through crowns in the canopy. GORT has been used to model the physical aspects of discontinuous plant canopies such as gap fraction, radiation transmission, and bi-directional

reflectance (Ni et al., 1999; Ni et al., 1997; Xin et al., 2012), and has been validated under a variety of environmental conditions (Liu et al., 2008). Recent efforts have been made to develop and evaluate a simplified GORT model for the use in coupled global dynamic terrestrial ecosystem models (Ni-Meister et al., 2010; Yang et al., 2010). Despite these successful applications, the current version of the GORT model does not have analytical solutions for radiation absorption by sunlit and shaded leaves, though previous studies have tried to solve the process of multiple scattering between canopy and background in an iterative manner (Song et al., 2009). However, sunlit and shaded leaves must be treated separately in photosynthesis modeling because flux densities of photosynthetically active radiation (PAR) incident on leaf surfaces are different (He et al., 2013). It is also necessary to integrate vertically over the canopy to derive mean PAR absorbed by sunlit and shaded leaves because of the non-linear light attenuation within the canopy and the non-linear dependence of leaf stomatal conductance on light absorption (Campbell and Norman, 1998).

The objectives of this study are to 1) advance the GORT model by providing analytical solutions to the radiation absorption of sunlit and shaded leaves and 2) link the radiative transfer process to biochemical processes to simulate leaf and canopy photosynthesis. We first describe the principles of our model and then perform model validation with eddy covariance data from two flux towers situated in the New England region of the United States.

2. Theoretical Basis

2.1 Brief description of canopy gap probability modeled using GORT

Gap probability, the probability of photons reaching a given canopy depth without being intercepted by canopy elements, is key to characterizing the radiation distribution within plant canopies. A detailed description for modeling the gap probability with GORT is described in previous studies (Li et al., 1995; Ni et al., 1999), and we summarize it briefly here because the concept of gap probability is necessary for understanding our subsequent work.
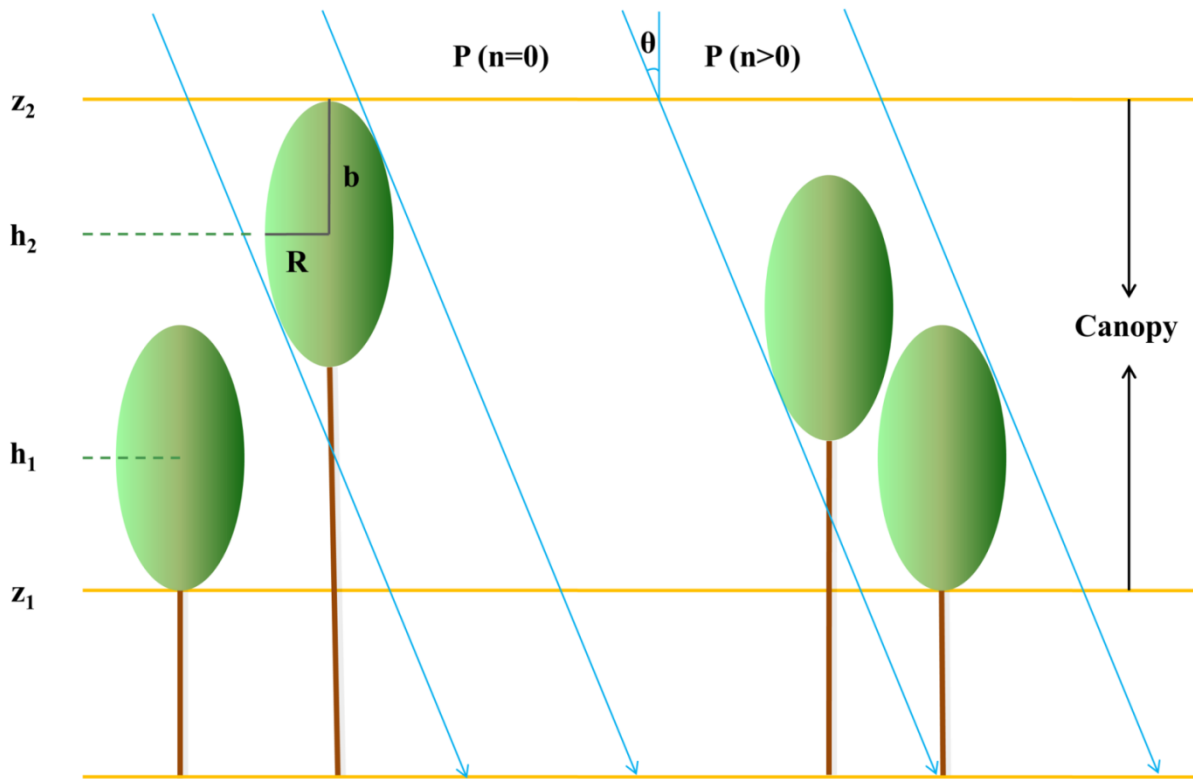
Figure 1: A scheme of the canopy structure in the Geometric Optical Radiative Transfer model as modified from Ni (1998).

For homogeneous canopies, Beer's law describes the gap probability of sunlight penetration. For discontinuous plant canopies, leaves are clumped within individual canopy crowns, forming an uneven distribution of gap probabilities for beam radiation. GORT models tree crowns as a collection of ellipsoids (Figure 1), of which the centers are randomly distributed between the upper and lower boundaries of the canopy layer (h_1 and h_2). Each ellipsoid, or each canopy crown, is characterized by one-half of the vertical crown length (b) and a horizontal crown radius (R). The total gap probability is modeled separately as the proportion of sunlight passing through the canopy layer without reaching any crown (hereafter referred to as between-crown gaps) and the proportion of sunlight passing through crowns without being intercepted by canopy leaves (hereafter referred to as within-crown gaps), such that:

$$P_{\text{gap}}(h, \theta_i) = P_{\text{gap}}(n = 0 | h, \theta_i) + P_{\text{gap}}(n > 0 | h, \theta_i) \tag{1}$$

6

126   where $P_{\text{gap}}(h, \theta_i)$ is the gap probability for beam radiation at height h given an illumination zenith angle θ_i,

127      $P_{\text{gap}}(n = 0|h, \theta_i)$ is the between-crown gap, and $P_{\text{gap}}(n > 0|h, \theta_i)$ is the within-crown gap.

128

129   The between-crown gap is modeled based on Boolean theory as an exponential function of crown numbers

130   within a geometric volume that contains no crown centers:

$$P_{\text{gap}}(n = 0|h, \theta_i) = e^{-\lambda_v V_\Gamma} \tag{2}$$

131   where λ_v is the tree density, and V_Γ is the beam projected cylinder volume with a radius R starting from the

132   canopy top and extending to height h.

133

134   Assuming that leaves are randomly distributed within each individual crown, the within-crown gap is

135   modeled based on Beer's law as light penetration along the traveling path length, such that:

$$P_{\text{gap}}(n > 0|h, \theta_i) = \int_0^\infty P(s|h, \theta_i) e^{-\tau(\theta_i)s} ds \tag{3}$$

136   where $\tau(\theta_i, \alpha) = k_b(\theta_i, \alpha) \cdot FAVD$, $FAVD$ is the foliage area volume density within a single crown, and

137      $k_b(\theta_i, \alpha)$ is the extinction coefficient for beam radiation given a specific solar illumination angle θ_i and leaf

138   distribution angle α. For a spherical leaf angle distribution, $k_b = \frac{0.5}{\cos(\theta_i)}$. $P(s|h, \theta_i)$ is the probability

139   distribution function associated with within-crown path length s.

140

141   The probability distribution of within-crown paths length can be solved in a convolutional manner:

$$P(s|h, \theta_i) = \int_h^{h_2} \sum_{n=1}^{n=\infty} P(s|n, z, h, \theta_i) P(n|z, h, \theta_i) \, dz \tag{4}$$

142   where $P(s|n, z, h, \theta_i)$ is the probability distribution of within-crown path length given that a solar ray enters

143   the crown at height h and angle θ_i, and $P(n|z, h, \theta_i)$ is the probability distribution of the numbers of crowns

144   intercepted by the solar ray incident at angle θ_i, entering crowns at height z, and then traveling to height h.

145

Diffuse radiation (i.e., the hemispherically isotropic radiation) can be treated as beam radiation from all directions in the upper hemisphere. The "openness" of discontinuous plant canopies to diffuse radiation on a horizontal plane is defined as:

$$K_{open}(h) = K_{open}(n = 0|h) + K_{open}(n > 0|h) \tag{5}$$

$$K_{open}(n = 0|h) = \frac{1}{\pi} \int_0^{2\pi} \int_0^{\frac{\pi}{2}} P_{gap}(n = 0|h, \theta_i) \sin(\theta_i) \cos(\theta_i) d\theta_i d\phi$$

$$= 2 \int_0^{\frac{\pi}{2}} P_{gap}(n = 0|h, \theta_i) \sin(\theta_i) \cos(\theta_i) d\theta_i \tag{6}$$

$$K_{open}(n > 0|h) = \frac{1}{\pi} \int_0^{2\pi} \int_0^{\frac{\pi}{2}} P_{gap}(n > 0|h, \theta_i) \sin(\theta_i) \cos(\theta_i) d\theta_i d\phi$$

$$= 2 \int_0^{\frac{\pi}{2}} P_{gap}(n > 0|h, \theta_i) \sin(\theta_i) \cos(\theta_i) d\theta_i \tag{7}$$

where $K_{open}(n = 0|h)$ and $K_{open}(n > 0|h)$ are between-crown and within-crown openness factors, respectively. θ_i is the solar illumination angle, and ϕ is the azimuth angle.

151

2.2 Sunlit and shaded leaf area index

The gap probability describes the probability of beam radiation being intercepted by plant leaves, and hence determines the proportion of leaf areas that are sunlit. For a very thin layer, the reduction of total gap probability is due to leaf interception, of which the process still follows Beer's law:

$$P_{gap}(h - \delta h, \theta_i) = \exp(-k_b \delta LAI(h)) P_{gap}(h, \theta_i) \tag{8}$$

where k_b is the canopy extinction coefficient for beam irradiance, $\delta LAI(h)$ is the leaf area index within a thin layer δh at height h, and $P_{gap}(h, \theta_i)$ is the gap probability modeled using GORT.

158

In the limit as δh becomes infinitely small, we have:

$$\exp(-k_b \delta LAI(h)) = 1 - k_b \delta LAI(h) \tag{9}$$

$$P_{\text{gap}}(h - \delta h, \theta_i) = P_{\text{gap}}(h, \theta_i) - P'_{\text{gap}}(h, \theta_i)\delta h \tag{10}$$

where $P'_{\text{gap}}(h, \theta_i)$ is the first derivative of gap probability $P_{\text{gap}}(h, \theta_i)$ with respect to height h.

Combining Equations (8), (9), and (10), we obtain:

$$\frac{P'_{\text{gap}}(h, \theta_i)}{P_{\text{gap}}(h, \theta_i)} \delta h = k_b \delta LAI(h) \tag{11}$$

For diffuse radiation, it can be derived in a similar manner:

$$\frac{K'_{\text{open}}(h)}{K_{\text{open}}(h)} \delta h = k_d \delta LAI(h) \tag{12}$$

where k_d is the extinction coefficient for diffuse irradiance, and $K'_{\text{open}}(h)$ is the first derivative of the openness factor $K_{\text{open}}(h)$ with respect to height h.

The sunlit LAI at height h is the product of the probability of beam sunlight penetration to height h and the probability of sunlight being intercepted by the thin layer and divided by the ratio of leaf area projected on a horizontal surface (Campbell and Norman, 1998), such that:

$$\delta LAI_{Sun}(h, \theta_i) = \frac{P_{\text{gap}}(h, \theta_i)\left[1 - \exp(-k_b \delta LAI(h))\right]}{k_b} \tag{13}$$

where $\delta LAI_{Sun}(h, \theta_i)$ is the sunlit leaf area index within a thin layer δh at height h.

Substituting Equations (9) and (11) into Equation (13), we obtain:

$$\delta LAI_{Sun}(\theta_i) = \frac{P'_{\text{gap}}(h, \theta_i)}{k_b} \delta h \tag{14}$$

Sunlit LAI for the entire canopy at zenith angle θ is then obtained by integrating from the canopy top to canopy bottom, such that:

$$LAI_{Sun}(\theta_i) = \int_{z_1}^{z_2} \frac{P'_{\text{gap}}(h, \theta_i)}{k_b} dh = \frac{1 - P_{\text{gap}}(h = z_1 | \theta_i)}{k_b} \tag{15}$$

where $P_{\text{gap}}(h = z_2 | \theta_i)$ and $P_{\text{gap}}(h = z_1 | \theta_i)$ are the gap probabilities at the canopy top z_2 and canopy bottom z_1, respectively, whereas the gap probability at the canopy top is 1.

It is worth noting that our calculation of sunlit leaf area for discontinuous canopies is analogous to that for homogeneous canopies, which is given as:

$$LAI^*_{Sun}(\theta_i) = \int_0^{LAI} \exp(-k_b \cdot L) \, dL = \frac{1 - \exp(-k_b \cdot LAI)}{k_b} \tag{16}$$

where $LAI^*_{Sun}(\theta_i)$ is the sunlit leaf area for homogeneous canopies.

The shaded LAI is simply the remainder of the canopy LAI:

$$LAI_{Shd} = LAI - LAI_{Sun} \tag{17}$$

2.3 Analytical solutions for the scattering parameters of discontinuous canopies

Canopy scattering parameters such as directional-hemispherical reflectance and hemispherical-hemispherical reflectance (or black-sky albedo and white-sky albedo, respectively) can be obtained by resolving the radiative transfer process or can be approximated using simple analytical solutions. For semi-infinite horizontally homogeneous media, Hapke's solutions of the proportion of unintercepted direct beam ($t_0(h, \theta_i)$), hemispherical-hemispherical reflectance (R_{ff}^∞), directional-hemispherical reflectance (R_{df}^∞),

hemispherical-hemispherical transmittance (T_{ff}^∞), and directional-hemispherical transmittance (T_{df}^∞) are given as (Hapke, 1981):

$$t_0(h, \theta_i) = e^{-\frac{\tau(\theta_i)h}{\mu_i}} \tag{18}$$

$$R_{ff}^\infty = \frac{1-\gamma}{1+\gamma} \tag{19}$$

$$R_{df}^\infty(\theta_i) = \frac{1-\gamma}{1+2\mu_i\gamma} \tag{20}$$

$$T_{ff}^\infty(h) = e^{-2\gamma\tau h} \tag{21}$$

$$T_{df}^\infty(h, \theta_i) = \frac{\sigma}{2} \frac{1+2\mu_i}{1-(2\mu_i\gamma)^2} [T_{ff}^\infty(h) - t_0(h, \theta_i)] \tag{22}$$

where σ is the single scattering albedo, $\tau = k(\theta_i)\frac{L_e}{H}$ is the projected foliage area volume density for the plant canopy, L_e is the effective leaf area index, H is the depth of the canopy, θ_i is the solar illumination angle, $\mu_i = \cos(\theta_i)$ and $\gamma = \sqrt{1-\sigma}$.

Starting with surface energy balances, Ni (1998) derived the scattering parameters for a horizontally homogeneous canopy layer with finite thickness as:

$$t_{ff}(h) = T_{ff}^\infty(h) \frac{1-(R_{ff}^\infty)^2}{1-(T_{ff}^\infty(h)R_{ff}^\infty)^2} \tag{23}$$

$$\rho_{ff}(h) = R_{ff}^\infty(h) \frac{1-(T_{ff}^\infty(h))^2}{1-(T_{ff}^\infty(h)R_{ff}^\infty)^2} \tag{24}$$

$$t_{df}(h, \theta_i) = T_{df}^\infty(h, \theta_i) - \rho_{ff}(h)[t_0(h, \theta_i)R_{df}^\infty(\theta_i) + T_{df}^\infty(h, \theta_i)R_{ff}^\infty] \tag{25}$$

$$\rho_{df}(h, \theta_i) = R_{df}^\infty(h) - t_{ff}(h)[t_0(h, \theta_i)R_{df}^\infty(\theta_i) + T_{df}^\infty(h, \theta_i)R_{ff}^\infty] \tag{26}$$

where $t_{ff}(h)$, $\rho_{ff}(h)$, $t_{df}(h,\theta_i)$, and $\rho_{df}(h,\theta_i)$ are hemispherical-hemispherical transmittance, hemispherical-hemispherical reflectance, directional-hemispherical transmittance, and directional-hemispherical reflectance, respectively.

The scattering parameters for a discontinuous canopy can then be approximated as combinations of a homogeneous vegetation layer and a non-vegetated layer:

$$t'_{ff}(h) = t_{ff}(h)\left(1 - K_{\text{open}}(n = 0|h)\right) + K_{\text{open}}(n = 0|h) \tag{27}$$

$$\rho'_{ff}(h) = \rho_{ff}(h)\left(1 - K_{\text{open}}(n = 0|h)\right) \tag{28}$$

$$t'_{df}(h,\theta_i) = t_{df}(h,\theta_i)\left(1 - P_{\text{gap}}(n = 0|h,\theta_i)\right) + P_{\text{gap}}(n = 0|h,\theta_i) \tag{29}$$

$$\rho'_{df}(h,\theta_i) = \rho_{df}(h,\theta_i)\left(1 - P_{\text{gap}}(n = 0|h,\theta_i)\right) \tag{30}$$

where $t'_{ff}(h)$, $\rho'_{ff}(h)$, $t'_{df}(h,\theta_i)$, and $\rho'_{df}(h,\theta_i)$ are hemispherical-hemispherical transmittance, hemispherical-hemispherical reflectance, directional-hemispherical transmittance, and directional-hemispherical reflectance, respectively. Note that our equations here are slightly different from those used by Ni et al. (1999) because between-crown gaps, within which light attenuation obeys Beer's law, are considered in the homogeneous vegetation layer.

The analytical approximation of the canopy reflectance for beam and diffuse radiation is the sum of three factors in radiative transfer: the incoming irradiance scattered by the canopy elements, the first-order scattered radiation from soil background, and the irradiance scattered back and forth between the canopy layer and background surface (Ni et al., 1999). Taking beam radiation as an example and assuming that the background surface is Lambertian, the incoming irradiance scattered by the canopy elements is ρ'_{df}, the first-order scattered radiance from soil background is $t'_{df}\rho_s t'_{ff}$, and the multiple scattering between the

12

218 canopy elements and soil background is $t'_{df}\left(\rho_s\rho'_{ff}\rho_s + \rho_s(\rho'_{ff}\rho_s)^2 + \rho_s(\rho'_{ff}\rho_s)^3 + \cdots\right)t'_{ff}$. The canopy

219 reflectance for beam irradiance can then be written as:

$$
\begin{aligned}
\rho_{cb} &= \rho'_{df} + t'_{df}\left(\rho_s + \rho_s\rho'_{ff}\rho_s + \rho_s(\rho'_{ff}\rho_s)^2 + \rho_s(\rho'_{ff}\rho_s)^3 + \cdots\right)t'_{ff} \\
&= \rho'_{df} + t'_{df}\frac{\rho_s}{1 - \rho_s\rho'_{ff}}t'_{ff}
\end{aligned}
\tag{31}
$$

220

221 The canopy reflectance for diffuse irradiance can be obtained similarly as:

$$
\rho_{cd} = \rho'_{ff} + t'_{ff}\frac{\rho_s}{1 - \rho_s\rho'_{ff}}t'_{ff}
\tag{32}
$$

222

223 **2.4 Mean photosynthetically active radiation absorbed by sunlit and shaded leaves**

224 Let I_0 be the flux density of incoming solar radiation on a horizontal plane at the top of the canopy and f_b be

225 the fraction of incident beam radiation, the unintercepted beam and diffuse fluxes are then:

$$
I_b(h, \theta_i) = P_{\text{gap}}(h, \theta_i)(1 - \rho_{cb})f_b I_0 k_b
\tag{33}
$$

$$
I_d(h) = K_{\text{open}}(h)(1 - \rho_{cd})(1 - f_b)I_0 k_d
\tag{34}
$$

226 where ρ_{cb} and ρ_{cd} are canopy reflectance for beam and diffuse irradiance, respectively; I_b and I_d are the

227 unintercepted beam and diffuse fluxes, respectively; and k_b and k_d are canopy extinction coefficients for

228 beam and diffuse irradiance, respectively.

229

230 The downward beam flux I_b is derived based on the assumption of black leaves, meaning that leaves absorb

231 incident irradiance completely and do not transmit radiation (Bonan, 2002). To account for the effects of

232 leaf scattering, the total beam I_{bt} (i.e., unintercepted beam and down scattered beam) and total diffuse I_{dt}

233 (i.e., unintercepted diffuse and down scattered diffuse) irradiance can be modeled by introducing a factor of

234 $\sqrt{1 - \sigma}$ to extinction coefficients similar to the two-stream radiative transfer model (Sellers, 1985). As

235   single scattering albedo increases, the effective extinction coefficient becomes smaller and more sunlight is

236   allowed to transmit through the canopy. That is:

$$I_{bt}(h, \theta_i) = P_{\text{gap}}(h, \theta_i)^{\sqrt{1-\sigma}}(1 - \rho_{cb})f_b I_0\sqrt{1-\sigma}k_b \tag{35}$$

$$I_{dt}(h) = K_{\text{open}}(h)^{\sqrt{1-\sigma}}(1 - \rho_{cd})(1 - f_b)I_0\sqrt{1-\sigma}k_d \tag{36}$$

237   where σ is the single scattering albedo of leaves. $\sigma = \rho_l + t_l$, where ρ_l and t_l are leaf reflectance and

238   transmittance, respectively.

239

240   The total irradiance absorbed by the entire canopy per unit ground area consists of leaf absorption for both

241   beam and diffuse irradiance:

$$I_c = I_{cb} + I_{cd} = \int_0^{LAI} I_{bt}(h, \theta_i)dL + \int_0^{LAI} I_{dt}(h, \theta_i)dL \tag{37}$$

242

243   Substituting Equations (11), (12), (35), and (36) into Equation (37), we have:

$$I_{cb} = \int_{z_1}^{z_2} P_{\text{gap}}(h, \theta_i)^{\sqrt{1-\sigma}}(1 - \rho_{cb})f_b I_0\sqrt{1-\sigma}\frac{P'_{\text{gap}}(h, \theta_i)}{P_{\text{gap}}(h, \theta_i)}dh$$

$$= \left(1 - P_{\text{gap}}(h = z_1| \theta_i)^{\sqrt{1-\sigma}}\right)(1 - \rho_{cb})f_b I_0 \tag{38}$$

$$I_{cd} = \int_{z_1}^{z_2} K_{\text{open}}(h)^{\sqrt{1-\sigma}}(1 - \rho_{cd})(1 - f_b)I_0\sqrt{1-\sigma}\frac{K'_{\text{open}}(h)}{K_{\text{open}}(h)}dh$$

$$= \left(1 - K_{\text{open}}(h = z_1)^{\sqrt{1-\sigma}}\right)(1 - \rho_{cd})(1 - f_b)I_0 \tag{39}$$

244

245   Irradiance absorbed by sunlit leaves per unit ground area is obtained as the sum of direct beam, downward

246   scattered beam, and diffuse components:

$$I_{Sun} = I_{Sunb} + I_{Sunbs} + I_{Sund} \tag{40}$$

247

14

248 Combining Equations (33), (35), (36), and (40), we have:

$$I_{Sunb} = \int_{z_1}^{z_2} (1-\sigma)f_b I_0 \cdot P'_{gap}(h,\theta_i)dh = (1-\sigma)\left(1 - P_{gap}(h=z_1|\theta_i)\right)f_b I_0 \qquad (41)$$

$$I_{Sunbs} = \int_{z_1}^{z_2} \left[P_{gap}(h,\theta_i)^{\sqrt{1-\sigma}}(1-\rho_{cb})\sqrt{1-\sigma} - P_{gap}(h,\theta_i)(1-\sigma)\right]f_b I_0 \cdot P'_{gap}(h,\theta_i)dh$$

$$= \left[\frac{\sqrt{1-\sigma}}{1+\sqrt{1-\sigma}}\left(1 - P_{gap}(h=z_1|\theta_i)^{1+\sqrt{1-\sigma}}\right)(1-\rho_{cb})\right. \qquad (42)$$

$$\left. - \frac{(1-\sigma)}{2}\left(1 - P_{gap}(h=z_1|\theta_i)^2\right)\right]f_b I_0$$

$$I_{Sund} = \int_{z_1}^{z_2} K_{open}(h)^{\sqrt{1-\sigma}}(1-\rho_{cd})(1-f_b)I_0\sqrt{1-\sigma}\cdot K'_{open}(h)dh$$

$$= \frac{\sqrt{1-\sigma}}{1+\sqrt{1-\sigma}}\left(1 - K_{open}(h=z_1)^{1+\sqrt{1-\sigma}}\right)(1-\rho_{cd})(1-f_b)I_0 \qquad (43)$$

249 Note that σ is used instead of ρ_{cd} for the beam irradiance of sunlit leaves because sunlit leaves scatter direct

250 beam sunlight only once.

251

252 The irradiance absorbed by shaded leaves per unit ground area is simply the difference between the total

253 irradiance absorbed by the canopy and the irradiance absorbed by sunlit leaves:

$$I_{Shd} = I_c - I_{Sun} \qquad (44)$$

254

255 The mean absorbed irradiance for sunlit and shaded canopy per leaf hemi-surface area is then:

$$Q_{Sun} = \frac{I_{Sun}}{LAI_{Sun}} \qquad (45)$$

$$Q_{Shd} = \frac{I_{Shd}}{LAI_{Shd}} \qquad (46)$$

256

15

2.5 Modeling leaf photosynthesis and scaling up to canopy photosynthesis

The biochemical process of carbon dioxide assimilation by leaves can be considered as a gas diffusion process through stomata. According to Fick's law, the process is described as:

$$A = g_c \cdot (C_a - C_i) \tag{47}$$

where A is the CO_2 assimilation rate, g_c is the stomatal conductance, and C_a and C_i are ambient and intercellular CO_2 concentrations, respectively.

Field studies have firmly established the relationship between leaf stomatal conductance and environmental conditions. Jarvis and McNaughton (1986) successfully synthesize the response functions in a multiple-constraint model:

$$g_c = g_{cmax} \prod f(x_i) \tag{48}$$

where g_{cmax} is the maximum leaf stomatal conductance when environmental factors do not limit carbon uptake and $f(x_i)$ are scalars that account for the influences of various environmental stresses on leaf stomatal conductance.

Different formulas have been developed to describe the response functions of photosynthesis to environmental factors. Here, we consider three main limiting factors imposed by radiation, temperature, and water on vegetation photosynthesis. The equations developed for the dual-source dual-leaf (DSDL) model (Ding et al., 2014), Terrestrial Ecosystem Model (Raich et al., 1991), and Biome-BGC models (Running et al., 2004) are used to account for the influences of radiation, temperature, and vapor pressure deficit (VPD), respectively:

$$\prod f(x_i) = f(Q) \cdot f(T) \cdot f(VPD) \tag{49}$$

$$f(Q) = \frac{k_C + k_Q}{k_Q} \cdot \frac{Q}{k_Q + Q} \qquad (50)$$

$$f(T) = \frac{(T - T_{min})(T - T_{max})}{(T - T_{min})(T - T_{max}) - (T - T_{opt})^2} \qquad (51)$$

$$f(VPD) = \frac{VPD_{max} - VPD}{VPD_{max} - VPD_{min}} \qquad (52)$$

276 where k_C and k_Q are the stress coefficients of PAR absorbed by plant leaves; Q is the mean APAR for sunlit

277 or shaded leaves per leaf hemi-surface area; T_{min}, T_{opt}, and T_{max} are the minimum, optimum, and

278 maximum temperature for photosynthetic activities, respectively; and VPD_{min} and VPD_{max} are the

279 minimum and maximum vapor pressure deficit, respectively. In the DSDL model, k_C and k_Q are 500 W/m²

280 and 150 W/m², respectively. T_{min}, T_{opt}, and T_{max} are determined as 10 °C, 28 °C and 48 °C for C4 crops

281 (Kalfas et al., 2011), and here we slightly lower their values to 0 °C, 25 °C, and 45 °C, respectively, for C3

282 plants. VPD_{min} and VPD_{max} are 0.65 kPa and 4.6 kPa for deciduous forests, respectively, in the Biome-

283 BGC model (Heinsch et al., 2003).

284

285 Due to different PAR absorption by sunlit and shaded leaves, the stomatal conductance for sunlit and shaded

286 leaves need to be calculated separately as:

$$g_{cSun} = g_{cmax} \cdot f(Q_{Sun}) \cdot f(T) \cdot f(VPD) \qquad (53)$$

$$g_{cShd} = g_{cmax} \cdot f(Q_{Shd}) \cdot f(T) \cdot f(VPD) \qquad (54)$$

287 where g_{cSun} and g_{cShd} are the stomatal conductance for sunlit and shaded leaves, respectively, and Q_{Sun}

288 and Q_{Shd} are the mean PAR absorbed by sunlit and shaded leaves, respectively.

289

290 Given measured ambient CO_2 concentrations, the closure of the formulation (47) now requires the quantity

291 of intercellular CO_2 concentrations. Katul et al. (2000) compared eight models and concluded that all

reproduced the measured carbon assimilation rates well. Here, we employ Leuning's method (Leuning, 1995) to estimate the ratio of intercellular to ambient CO_2 concentrations as:

$$\frac{C_i}{C_a} = 1 - \frac{1 - \frac{\Gamma}{C_a}}{m_L}\left(1 + \frac{VPD}{VPD_0}\right) \tag{55}$$

where VPD is the ambient vapor pressure deficit; VPD_0 is an empirical constant describing the species sensitivity to ambient vapor pressure deficit; Γ is the leaf CO_2 compensation point; C_a and C_i are ambient and intercellular CO2 concentrations, respectively; and m_L represents linear regression coefficients related to tree species. Calibrated values for model parameters are $m_L = 4.0$, $\Gamma = 40\ \mu mol/mol$, and $VPD_0 = 30\ kPa$, respectively (Katul et al., 2000).

Given modeled carbon assimilation rates at the leaf level, the total rate of carbon assimilation at the canopy level can be scaled up as:

$$GPP = A_{Sun} \cdot LAI_{Sun} + A_{Shd} \cdot LAI_{Shd} \tag{56}$$

where GPP is canopy gross primary production, A_{Sun} and A_{Shd} are leaf-level carbon assimilation rates for sunlit and shaded leaves, respectively, and LAI_{Sun} and LAI_{Shd} are the sunlit and shaded leaf area index.

3. Study materials and model parameterization

We studied two deciduous forest sites: Harvard Forest (US-Ha1) in Massachusetts and Bartlett Experimental Forest (US-Bar) in New Hampshire (Richardson et al., 2012). Basic information is briefly summarized in Table 1 for each site. Although plot layouts set up for the fieldwork did not match the exact footprints of flux towers (Yang et al., 2013), the measured tree structural attributes, such as tree density, are assumed to be representative of the two study sites.

313 Table 1. Site information as obtained from the AmeriFlux website unless notified.

Site code	Site name	Lat (°N)	Lon (°W)	Elevation (m)	Canopy height (m)	Tree density (trees/ha)[a]	Dominant species
US-Ha1	Harvard Forest	42.5378	72.1715	340	23.0	1020±72	red oak, red maple
US-Bar	Bartlett Experimental Forest	44.0646	71.2881	272	19.0	1432±67	American beech, red maple

314 [a] data from Yao et al. (2011)

315

316 Flux towers measure energy and material fluxes between ecosystem and the atmosphere continuously

317 (Baldocchi et al., 2001). Measured data are provided as standard Level 2 products in the AmeriFlux

318 database (http://ameriflux.ornl.gov/). The time steps of available data are half-hourly for US-Bar and hourly

319 for US-Ha1. The measurements we used include estimates of gross primary production (GPP) derived with

320 the eddy covariance technique (Baldocchi, 2003), and meteorological variables such as shortwave solar

321 radiation, temperature, vapor pressure deficit, and canopy-scale CO_2 concentration. Raw measurements of

322 meteorological variables were used for analysis and missing values due to instrument malfunction or

323 unsuitable micrometeorological conditions were screened. However, we obtained GPP estimates from

324 AmeriFlux Level 4 products if they were not delivered in Level 2 products. Extraterrestrial solar radiation

325 and solar zenith angle (i.e., the angle that the sun away from directly overhead) are calculated as a function

326 of geolocation (i.e., latitude and longitude), the day of year (DOY), and solar time of the day (Allen et al.,

327 1998). If diffuse radiation is missing from the measurements, we implement Muneer's method to partition

328 global solar radiation into beam and diffuse components (Muneer, 2007):

$$(1 - f_b) = 1.006 - 0.317K_t + 3.1241K_t^2 - 12.7616K_t^3 + 9.7166K_t^4 \tag{57}$$

329 where f_b is the proportion of beam radiation in global incoming radiation, and K_t is the hourly clearness

330 index. $K_t = I_0/I_e$, where I_0 is global solar radiation on the canopy top and I_e is the extraterrestrial solar

331 radiation.

332

333 We use typical parameter values from the literature for model parameterization. Because the spectral

334 signatures of vegetation leaves and soil background differ in the spectral bands of PAR and near infrared

335   (Table 2), we perform model simulations for these two discrete bands separately. Incident PAR is estimated

336   to account for 47.5% of incoming shortwave solar radiation, and the rest is attributed to the near infrared

337   band (Zhao et al., 2005). Maximum leaf stomatal conductance to H_2O is estimated as 5.5 mm/s for US-Bar

338   and 7.2 mm/s for US-Ha1 (Bonan, 2002; Ding et al., 2014), and they are translated to maximum leaf

339   stomatal conductance to CO_2 assuming that the temperature is 20°C and the atmospheric pressure is 101.32

340   kPa (Pearcy et al., 1989). Heights for canopy top (z_2) were measured to be 23.0 m for US-Ha1 and 19.0 m

341   for US-Bar (Table 1), and heights for canopy bottom (z_1) were estimated as $z_1 = 0.15\, z_z$. Canopy structure

342   in GORT is modeled with the ratios $H/b = 2.0$ and $b/R = 3.0$ (Strahler et al., 1999). Parameter values

343   defined for canopy structure are somewhat arbitrary but are identical to our previous modeling efforts (Liu

344   et al., 2008; Xin et al., 2012). The effects of tree structural parameters on model simulations are further

345   explored in our study by varying their values.

346

347   Table 2. The spectral signature of leaf and soil background.

Spectral bands	Leaf reflectance [a]	Leaf transmittance [a]	Soil reflectance [b]
Photosynthetic active radiation	0.10	0.05	0.23
Near infrared	0.45	0.25	0.32

348   [a] data from Bonan (2002)

349   [b] data from Myneni et al. (1995)

350

351   Model validation for vegetation photosynthesis is performed with time series data for 8 successive days and

352   for entire years. Based on AmeriFlux biological data, measured LAI were 4.7 $\pm$ 0.2 on DOY 211 in 2004 at

353   the US-Bar site and 4.84 $\pm$ 0.78 on DOY 234 in 2006 at the US-Ha1 site. Because field-measured LAI data

354   were insufficient to support model simulation for an entire calendar year, we obtained satellite-derived LAI

355   from the MODIS (Moderate Resolution Imaging Spectroradiometer) products (Myneni et al., 2002). The

356   standard MODIS products (MOD15A2) provide 8-day LAI estimates at 1000 m spatial resolution, and we

357   derived 8-day mean LAI for a 3 $\times$ 3 pixel window centered at each site. We screened cloudy observations

358   based on the Quality Control data in MOD15A2 and applied double logistic equations to fit time series of

359   cloud-free LAI observations (Li et al., 2014; Zhang et al., 2003).

360

4. Results

4.1 Gap probability

The gap probabilities derived from the GORT model are shown in Figure 2. As the solar zenith angle

increases, more beams of sunlight are intercepted by leaves and tree crowns, resulting in decreased gap

probabilities for both between- and within-crown gaps. As LAI increases, within-crown gaps decrease but

between-crown gaps remain the same. The physical explanation underlying is simple: tree leaves are

clumped within each individual crown such that variations in LAI would not affect between-crown gaps,

which are only a function of crown shape, canopy structure, and illumination geometry.

369

370
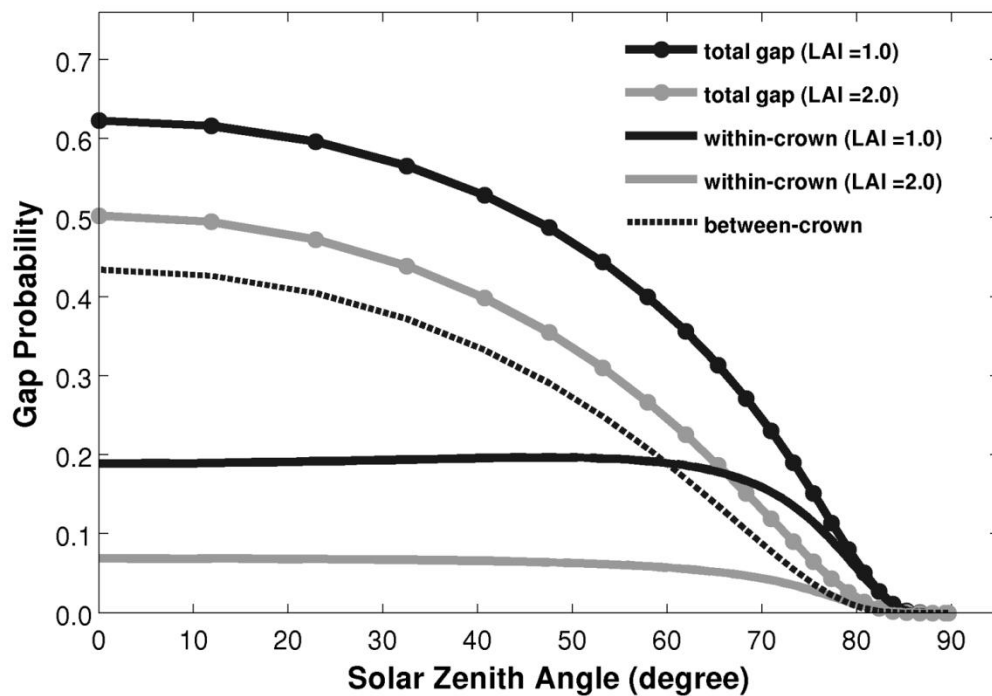
Figure 2: Canopy gap probabilities modeled using GORT with varied leaf area index. The total gaps are
between-crown gaps plus within-crown gaps. Tree structure parameters for the US-Bar site are used in
model simulation.

374

Figure 3 further compares the gap probabilities modeled using GORT and Beer's law. For both models, gap

probabilities decrease as solar zenith angle increases (Figure 3a). Modeled gap probabilities are close when

377   canopy LAI is low. However, at high LAI, the total gap derived from GORT is considerably greater than

378   that modeled using Beer's law due to strong clumping effects. With an LAI of 4.0, the differences in gap

379   probabilities are as much as 0.3 at the nadir, and in this case, more sunlight is allowed to transmit to the

380   ground surface in GORT than in classic radiative transfer models. Modeled vertical structures of sunlight

381   penetration are also shown to be different between GORT and Beer's law (Figure 3b). The gap probability

382   modeled using Beer's law decreases exponentially as canopy depth increases, whereas the decrease in the

383   GORT-modeled gap probability follows an inverse sigmoidal curve. The reason behind this can be

384   explained by the geometric factor: classic radiative transfer models assume that leaves are randomly

385   distributed within the canopy layer, but the GORT model assumes that leaves are randomly distributed

386   within individual crowns. Due to the ellipsoidal shape of tree crowns, there are simply more leaves in the

387   canopy center than near the canopy top and canopy bottom, where the gap probability decreases more

388   slowly.

389

390
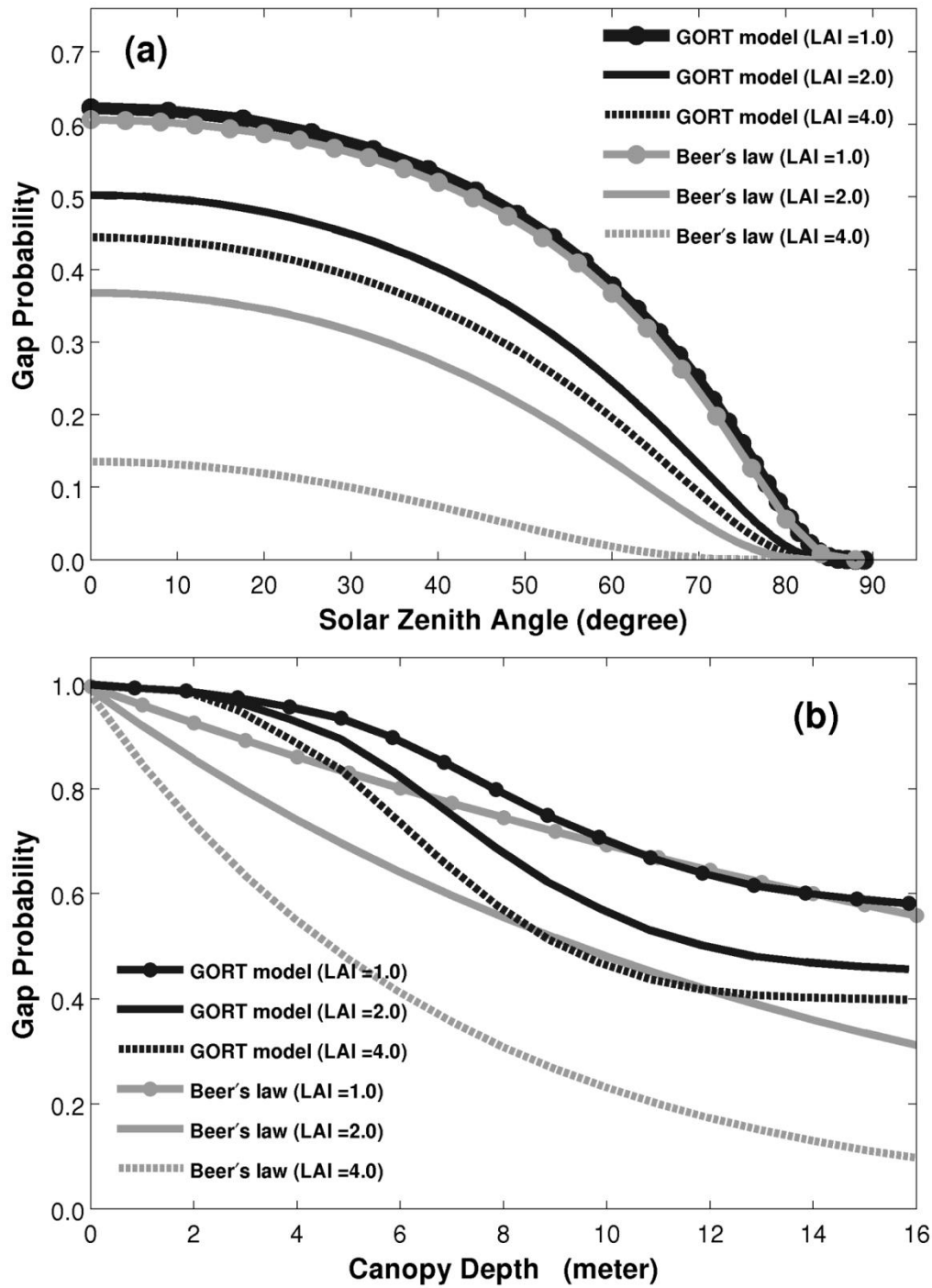
Figure 3: Comparisons between canopy gap probabilities modeled using GORT and Beer's law as a function of a) solar zenith angle and b) canopy depth. The canopy depth is defined as the distance from canopy top to a canopy height (h). Tree structure parameters for the US-Bar site are used in GORT simulation.

395

4.2 Model simulations over 8-day time periods

397   Figure 4 shows each component of the radiation regime at the US-Bar site. The diffuse radiation modeled

398   using Muneer's method matches flux tower measurements and accounts for 69.1% of the variances (Figure

399   4a). Because diffuse radiation was not measured at the US-Ha1 site, Muneer's method was implemented to

400   partition global radiation into diffuse and beam components for US-Ha1. Using the measured beam and

401   diffuse radiation, we simulate net radiation with GORT as a linear combination of two discrete bands at PAR

402   and near infrared. Modeled net radiation is highly correlated with measured values (R^2=0.981),

403   demonstrating the ability of GORT to model radiation absorption at the US-Bar site.

404

405
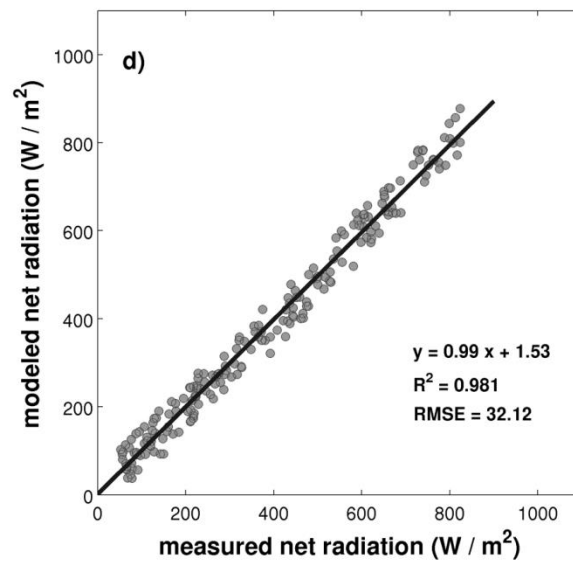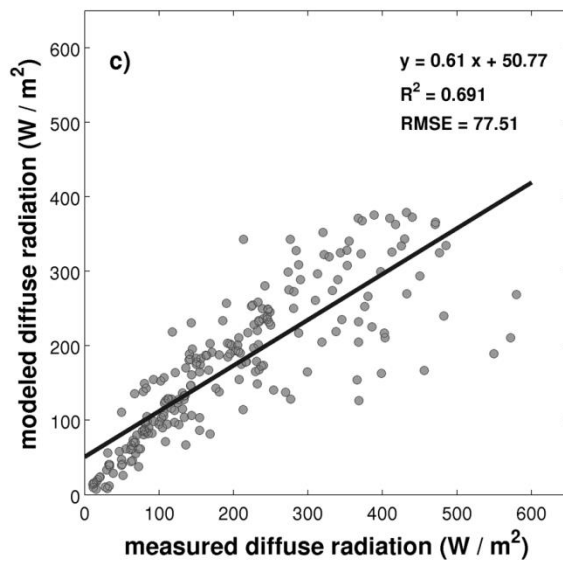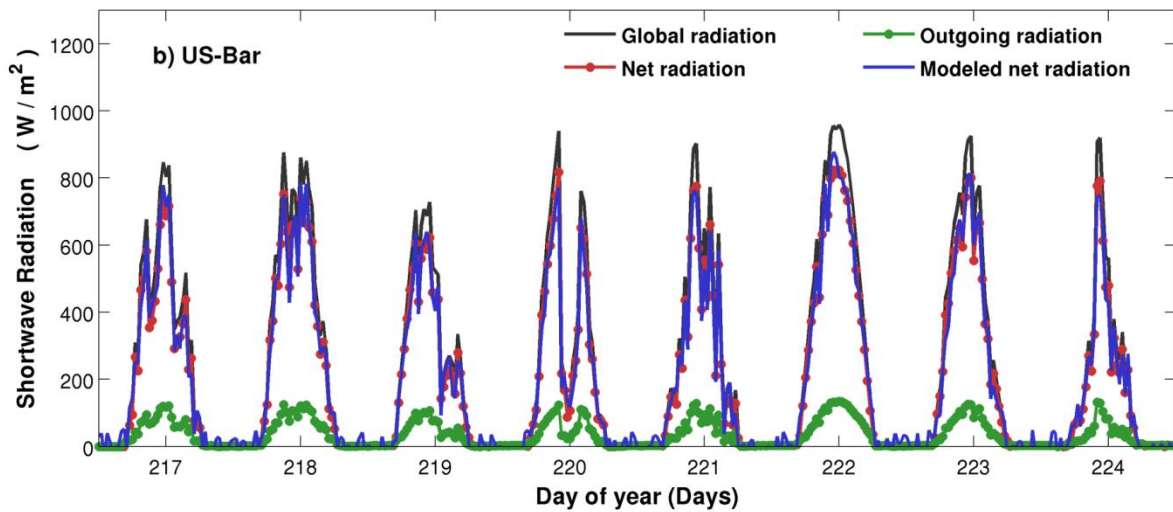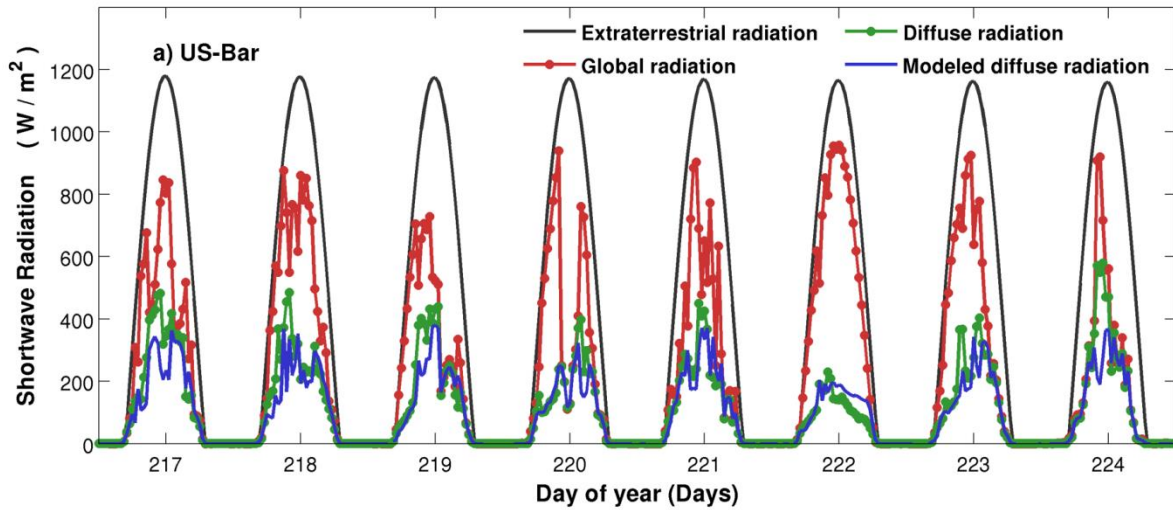
Figure 4: Measured and modeled components of radiation in 8 successive days are shown for a) the partition
of global solar radiation, b) surface radiation balance, c) modeled and measured diffuse radiation, and d)
modeled and measured net radiation. Extraterrestrial radiation is derived following methods outlined in

409 Allen et al. (1998). Muneer's method is applied to model diffuse radiation. The GORT model is applied to
410 model net radiation. Data are shown from the Day of Year 217 to 224 in 2004 for the US-Bar site.
411

412 Time series of each component for modeling canopy photosynthesis are shown in Figure 5. Given that total

413 LAI remains the same over the course of several days, modeled sunlit and shaded LAI have little day-to-day

414 variability and only vary as a function of solar zenith angle (Figure 5a). As solar zenith angle decreases,

415 sunlit LAI increases but shaded LAI decreases. Because sunlit leaves receive more illumination, they have

416 less radiation limitations on photosynthesis than shaded leaves (Figure 5b). Temperature limitation generally

417 decreases from morning until noon, while VPD limitation increases. Although the chemical process of

418 photosynthesis favors higher temperatures, leaf stomata tend to close to reduce water loss when atmospheric

419 dryness is high (Bonan, 2002). Because short-term canopy CO_2 concentrations vary with winds and

420 convection between the ecosystem and the atmosphere, the ambient CO_2 concentrations exhibit the greatest

421 variation from day to day (Figure 5b), so do the modeled differences between ambient and intercellular CO_2

422 concentrations.

423
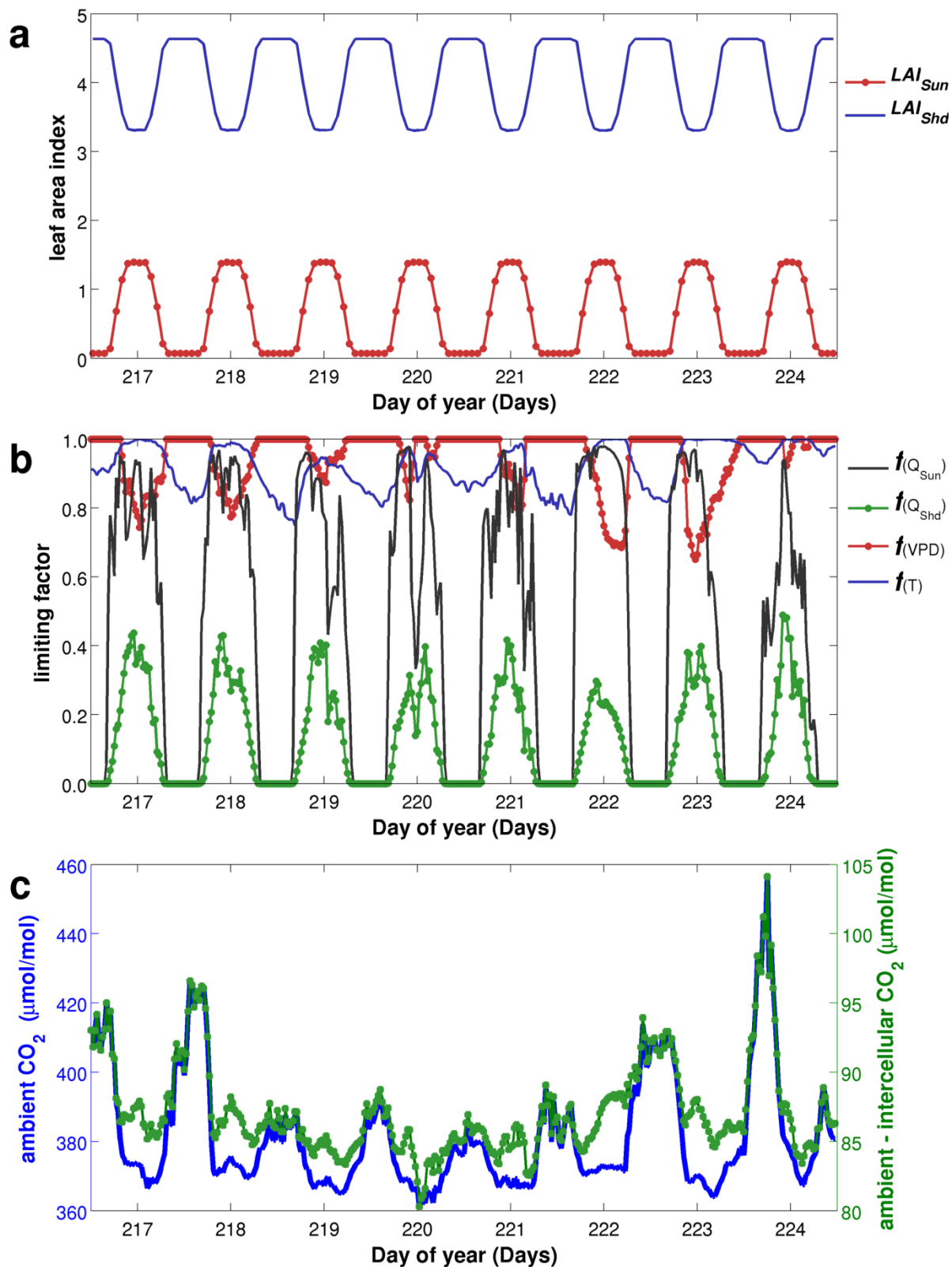
424

425 Figure 5: Time series of components of the photosynthesis calculation shown for a) sunlit and shaded leaf
426 area index, b) environmental limiting factors imposed by radiation absorption, temperature, and vapor
427 pressure deficit, and c) CO_2 concentration. Data are shown from the Day of Year 217 to 224 in 2004 for the
428 US-Bar site.

429

430   Figure 6 shows time series of measured and modeled GPP for two sites over eight successive days. GPP

431   estimates match flux tower measurements well in terms of the phase and amplitude. Daily peak GPP from

432   tower measurements are over 30.0 μmol CO_2 m^{-2} s^{-1} for both sites. It is also evident that modeled results can

433   capture some subtle variations in GPP at the hourly time scale. However, GPP estimates are slightly higher

434   on DOY 242 but lower on DOY 243 for US-Ha1. Note that we used Muneer's method for estimating the

435   diffuse radiation in US-Ha1 because measurements were not available. Considering uncertainties from the

436   partition of global solar radiation, results for both sites perform well in general.
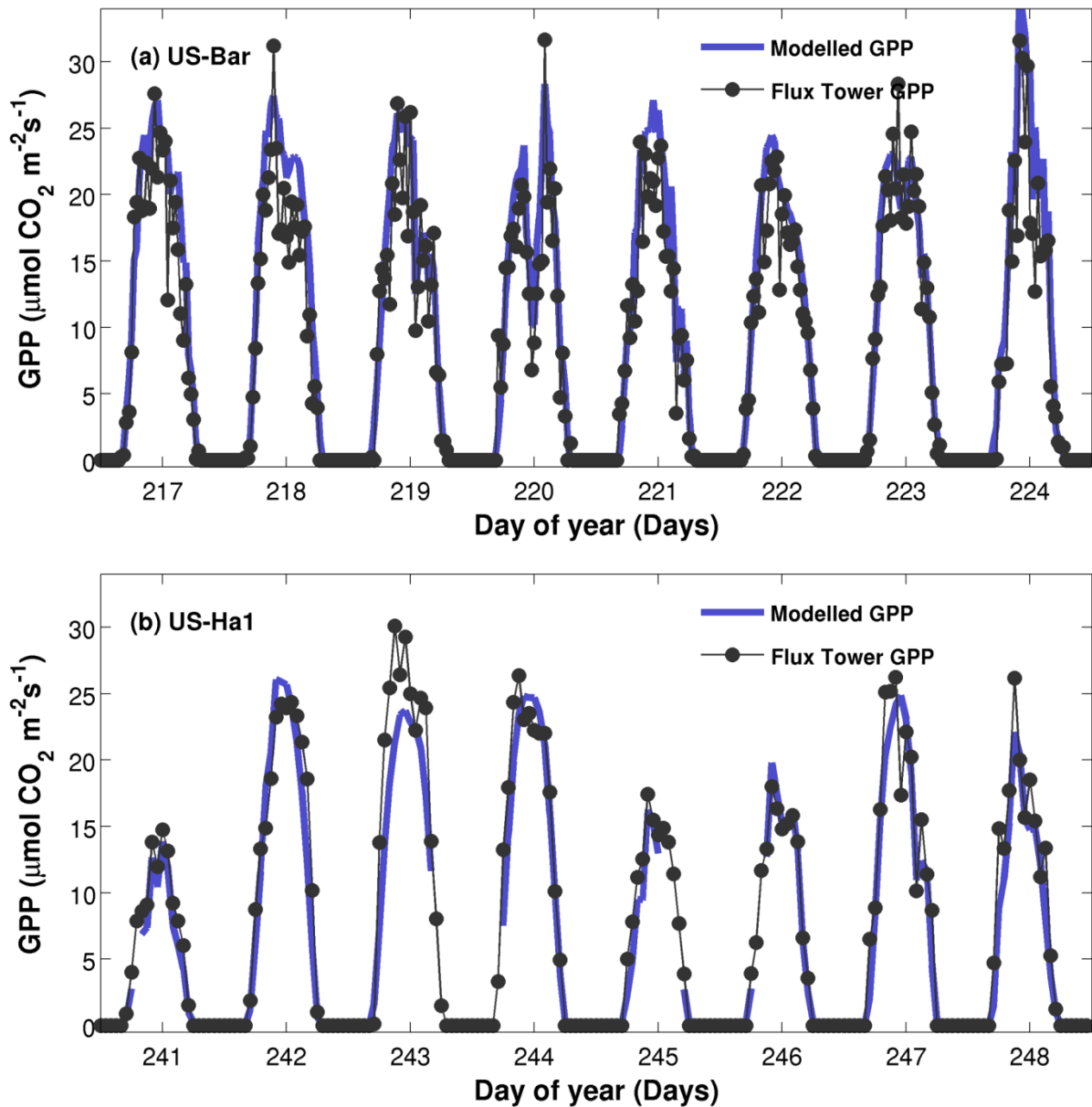
437

438 Figure 6: Time series of modeled and measured GPP for 8 consecutive days at the sites (a) US-Bar and (b)
439 US-Ha1. Data are half-hourly at the US-Bar site and hourly at the US-Ha1 site. Data are shown from DOY
440 217 to 224 in 2004 for US-Bar, and from DOY 241 to 224 in 2006 for US-Ha1. Negative GPP
441 measurements are set to zero. Missing points in modeled GPP at the US-Ha1 site are due to missing
442 measurement of canopy CO2 concentrations or other meteorological variables.
443

444 Figure 7 statistically compares measured and modeled GPP. Our model is able to explain 84.0% and 88.3%

445 of the GPP variances for the US-Bar and US-Ha1 sites, respectively. The regression lines are close to the 1 :

446 1 lines, and GPP is only slightly overestimated for US-Bar and underestimated for US-Ha1. The root mean

447 squared errors (RMSE) are 3.71 and 3.08 $\mu mol\ CO_2\ m^{-2}\ s^{-1}$ for US-Bar and US-Ha1, respectively. The

448 overall model performance is high considering that we did not attempt to perform model calibrations.

449
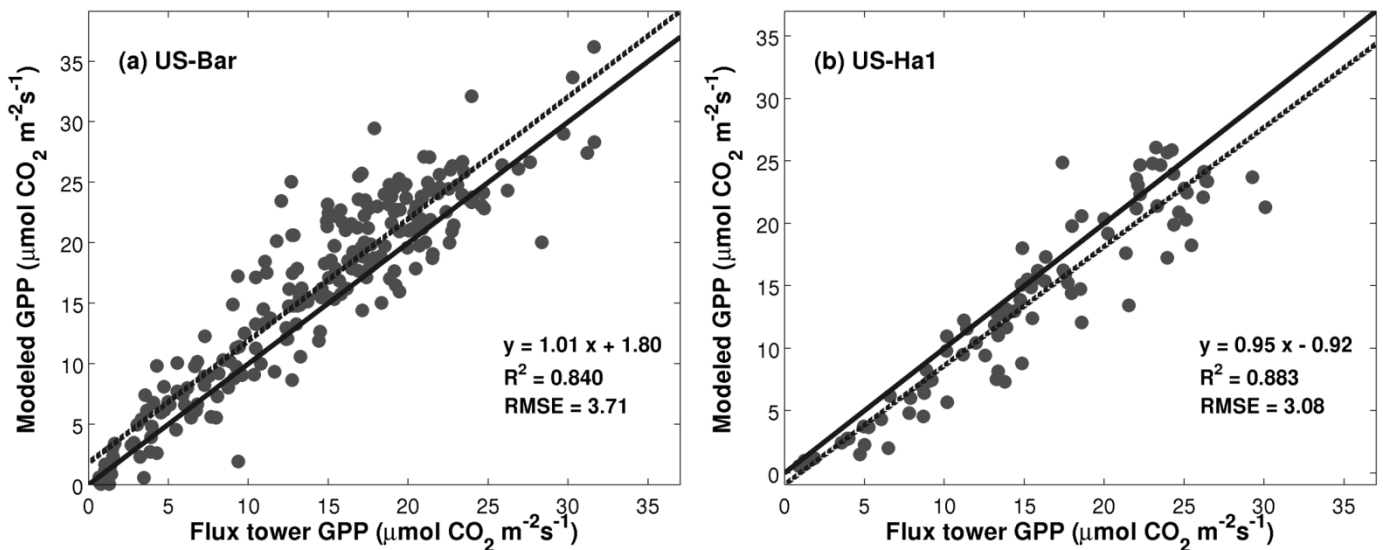
450

451 Figure 7: Regressions between modeled and measured GPP for 8 consecutive days at the sites (a) US-Bar
452 and (b) US-Ha1. Data are from DOY 217 – 224 in 2004 for US-Bar and from DOY 241 to 224 in 2006 for
453 US-Ha1. Only data during the photosynthetically active period (flux tower GPP > 0.5 $\mu mol\ CO_2\ m^{-2}\ s^{-1}$) are
454 included in the regression. The solid lines denote the 1 : 1 lines, and the dashed lines denote the regression
455 lines.
456

457 **4.3 Model simulation over entire years**

458 LAI derived from satellite observations (Figure 8) are used as inputs to model daily GPP over an entire year

459 in addition to the 8-day model simulations. The double logistic fitting lines are shown to reduce noises in

460 time series of MODIS LAI due to the effects of clouds and solar and viewing geometry. Fitted LAI time

29

461 series are slightly higher from June to August and lower from September to December in 2006 at the US-

462 Ha1 sites, but match with field measurements in general. The differences are likely to be introduced by

463 mismatched observation footprints and uncertainties in satellite retrieval algorithms. The fitted time series of

464 MODIS LAI are used for subsequent model simulations.

465

466
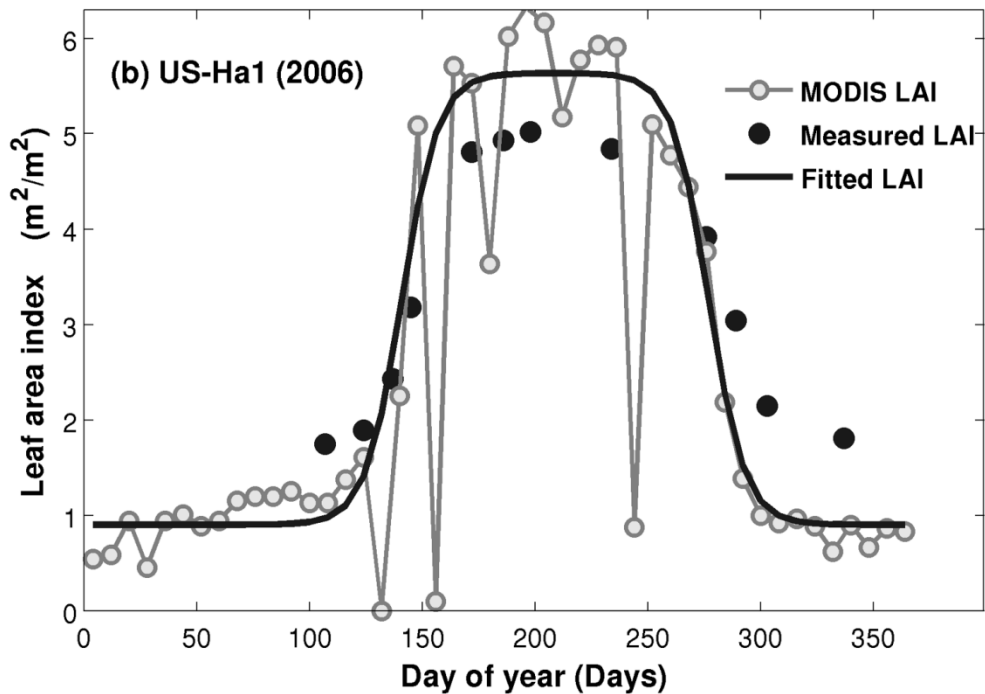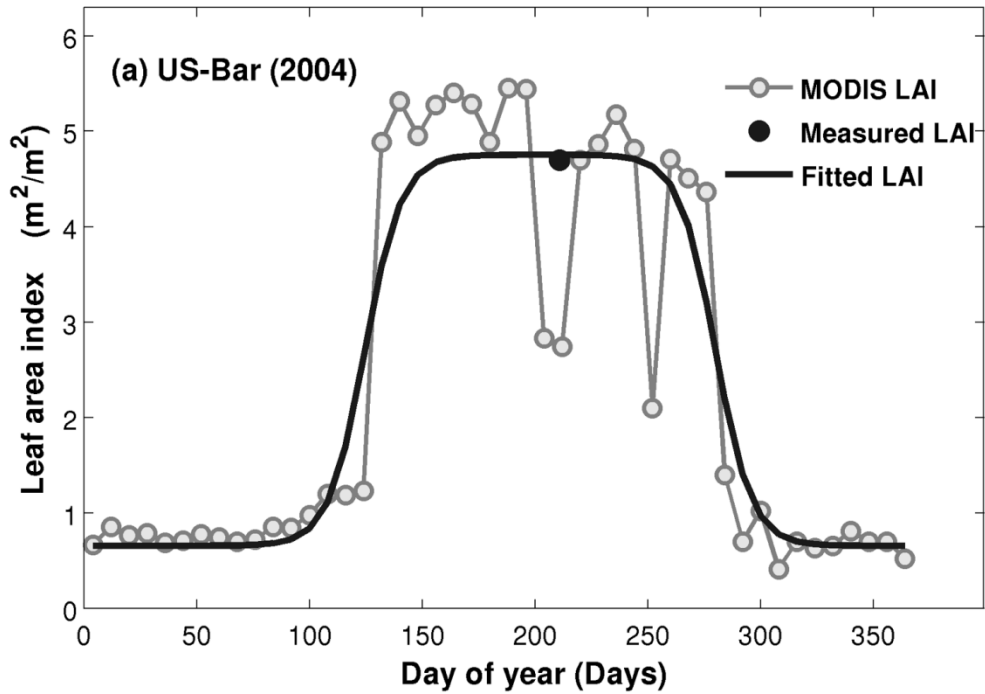
Figure 8: Comparisons of field-measured and satellite-derived leaf area indexes (LAI) for the sites a) US-Bar in 2004 and b) US-Ha1 in 2006. The solid grey lines denote MODIS LAI as obtained from standard MODIS FPAR/LAI products (MOD15A2). The solid black lines denote double logistic fitting lines that are applied to MODIS LAI. The solid points denote the measured LAI as obtained from biological datasets from AmeriFlux website.

Figure 9 presents time series of measured and modeled GPP at the US-Bar site. Modeled results capture the

trend and subtle variations of measured GPP on a daily basis. Most of the dips in the GPP time series occur

on cloudy days when radiation is the main limiting factor for vegetation photosynthesis. GPP values at US-

Bar are slightly overestimated from DOY 100 to 150 in 2004 possibly due to overestimation of the LAI.

Statistically, modeled results can explain 79.5%, 89.7%, and 89.3% of the variance in daily GPP for the

years 2004, 2005, and 2006, respectively (Figure 10). Regression slopes are close to the 1 : 1 lines except in

the year 2004 due to overestimated GPP in the early growing season. The RMSEs are 1.64, 1.31, and 1.56

gC m^{-2} day^{-1} for 2004, 2005, and 2006, respectively.

481
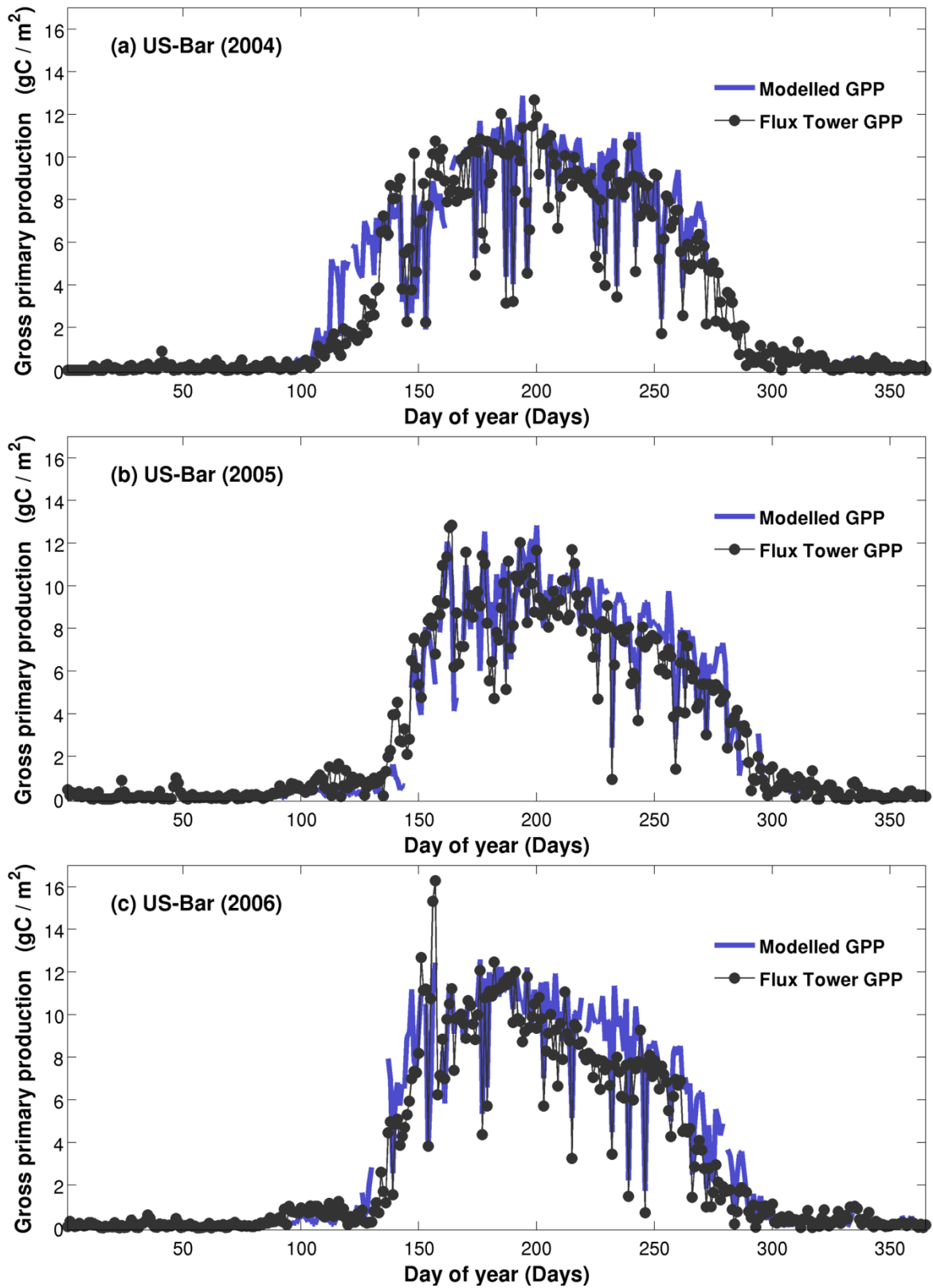
Figure 9: Time series of modeled and measured daily GPP shown for (a) 2004, (b) 2005, and (c) 2006 at the
US-Bar site. Model simulation is performed at a half-hourly time step. Measured and modeled half-hourly
GPP are aggregated to generate daily time series with units converted from μmol CO_2 m^{-2} s^{-1} to gC m^{-2} day^{-1}. Occational negative GPP measurements are set to zeros. Missing points in modeled GPP time series are

486 due to missing measurements of meteorological variables during the daytime photosynthetically active
487 period (flux tower GPP > 0.5 µmol CO_2 m^{-2} s^{-1}).
488
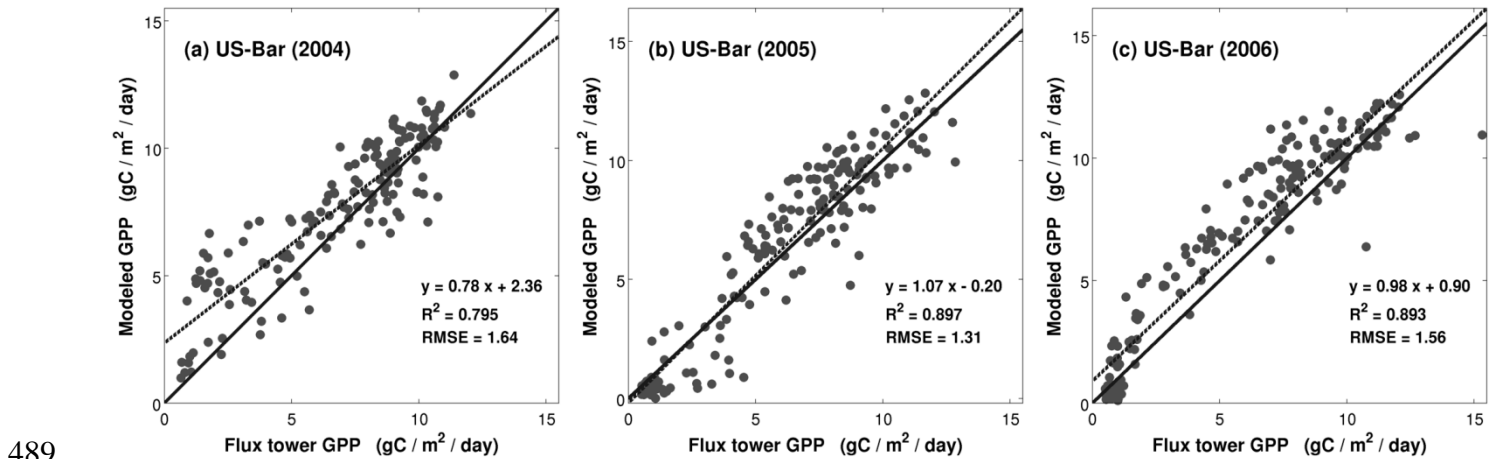
489

490 Figure 10: Regressions between modeled and measured daily GPP shown for (a) 2004, (b) 2005, and (c)
491 2006 at the US-Bar site. Only data during the photosynthetically active period (flux tower GPP > 0.5 gC m^{-2}
492 day^{-1}) are included in the regressions. The solid line denote the 1 : 1 lines, and the dashed lines denote the
493 regression lines.
494

495 Because measurements of atmospheric CO_2 concentrations within the canopy are largely unavailable for

496 US-Ha1 (only approximately 41.4% of the measurements are valid for use), we do not aggregate hourly

497 results to daily sums but perform regression analysis using all available hourly data in Figure 11. For the

498 US-Bar site, the R^2 value is 0.801 and the RMSE value is 4.31 µmol CO_2 m^{-2} s^{-1}. For the US-Ha1 site, the

499 correlation between modeled and measured GPP is strong with an R^2 value of 0.777 and an RMSE value of

500 6.49 µmol CO_2 m^{-2} s^{-1}. There were slight GPP underestimates when measured GPP values are high at the

501 US-Ha1 site, possibly due to empirical functions that we used in modeling diffuse radiation and leaf

502 photosynthesis. Table 3 lists major statistical results for our model performance, as evaluated using all

503 available hourly data at both sites. The model performance is consistent through time and is comparable to

504 the simulation of 8-day data (Figure 7), despite the fact that satellite-derived LAI instead of field

505 measurements were used for yearly simulation.

506

33
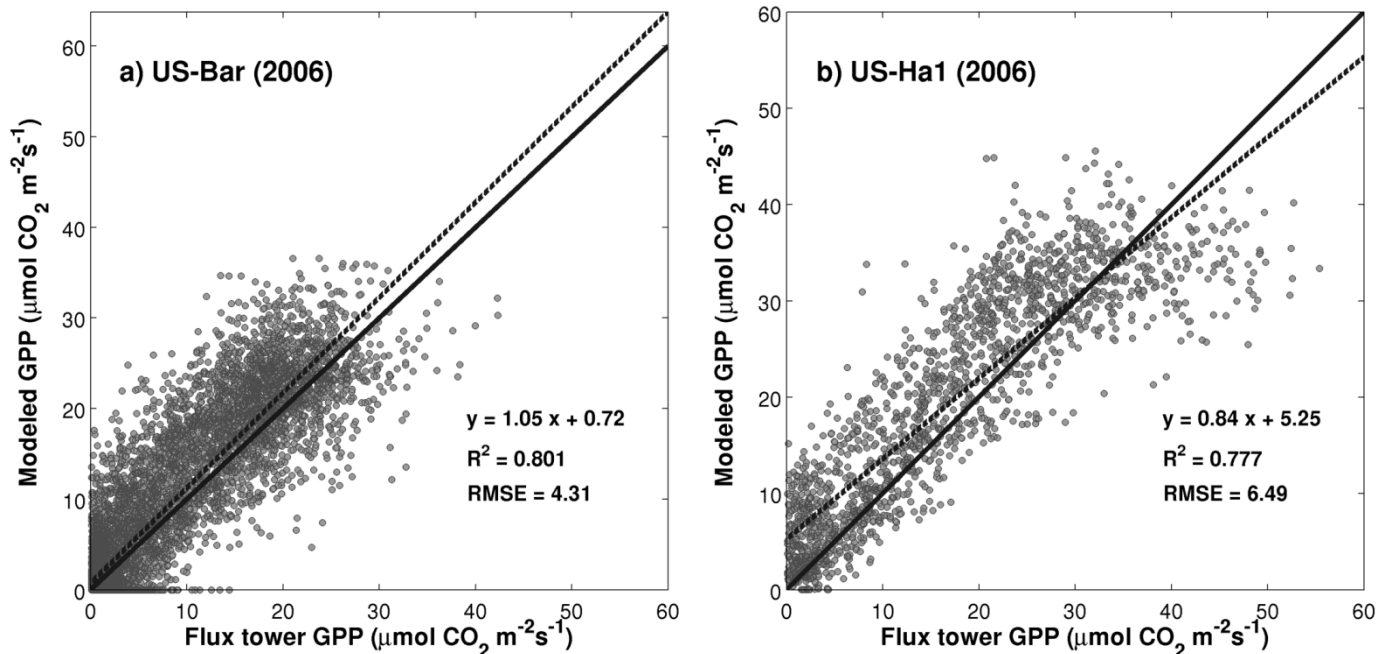
Figure 11: Regressions between modeled and measured GPP for all available hourly data at the sites of a) US-Bar and b) US-Ha1 in 2006. Only data from the photosynthetically active period are included in the regression. The solid line denotes the 1 : 1 line, and the dashed line denotes the regression line.

Table 3. The model performance at two study sites as evaluated using hourly data. Units for root mean square error (RMSE) and mean bias error (Bias) are in $\mu mol\ CO_2\ m^{-2}\ s^{-1}$.

| Year	US-Bar			US-Ha1		
	R^2	RMSE	Bias	R^2	RMSE	Bias
2001				0.804	5.44	2.00
2002				0.729	6.75	3.09
2003				0.781	5.62	2.85
2004	0.784	4.28	1.01	0.737	6.39	1.85
2005	0.795	4.11	0.47	0.736	6.83	1.18
2006	0.801	4.31	1.06	0.777	6.49	2.28
2007				0.768	6.21	2.50
2008				0.689	7.34	3.10
2009				0.662	7.62	3.68
2010				0.752	6.55	0.35
2011				0.715	6.96	1.34

5. Discussion

5.1 Influence of CO_2 concentration on canopy photosynthesis

One important question is whether it is necessary to link radiative transfer with leaf stomatal conductance

for modeling photosynthesis, since some biogeochemical models such as Production Efficiency Models

34

520 simply assume that vegetation GPP/NPP is linearly related to canopy radiation absorption (Xin et al., 2013).

521 To understand the performance of Production Efficiency Models, we conduct linear regressions between

522 modeled APAR and measured GPP as shown in Figure 12. Indeed, canopy APAR is positively related to flux

523 tower GPP and explains 70.3% of its variance. The R^2 value increases slightly to 0.710 after accounting for

524 the influences of temperature and vapor pressure. The model performance here is comparable to results from

525 other studies that evaluate Production Efficiency Models (Chen et al., 2011; Sjöström et al., 2013; Xin et al.,

526 2015).

527
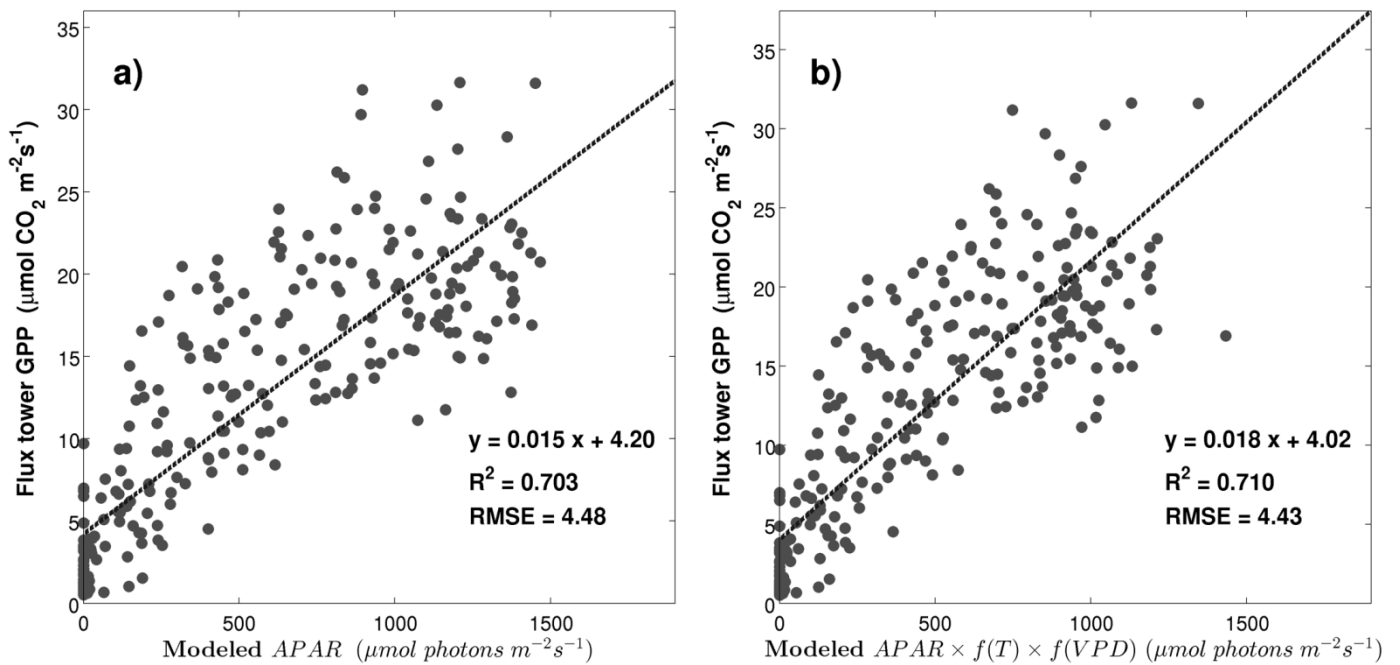
528

529 Figure 12: Regressions between modeled absorbed photosynthetic active radiation (APAR) and measured
530 GPP. Half-hourly data are shown from DOY 217 − 224 in 2004 for US-Bar. The influences of temperature
531 and vapor pressure deficit are modeled based on Equations (51) and (52). Only data during the
532 photosynthetically active period are included in the regression. The dashed lines denote the regression lines.
533

534 However, there are strong partial correlations between canopy CO2 concentrations and GPP even after

535 accounting for radiation absorption. Figure 13a shows the residual plot of GPP versus ambient CO2

536 concentrations when controlling on APAR. The slope is negative because the ambient CO2 concentration, as

537 regulated by vegetation photosynthesis and respiration activities, is normally high during the nighttime but

low during the daytime. The correlation coefficient is only -0.279, but it is statistically significant (p-value < 0.001) under a one-tailed partial correlation test. The data clearly allow rejection of the null hypothesis that ambient CO_2 concentration has no effects on canopy photosynthesis. This relationship holds even after considering the factors of temperature and vapor pressure deficit (Figure 13b). We therefore conclude that accounting for the influence of ambient CO_2 concentrations is essential for modeling daytime GPP at the half-hourly time scale.
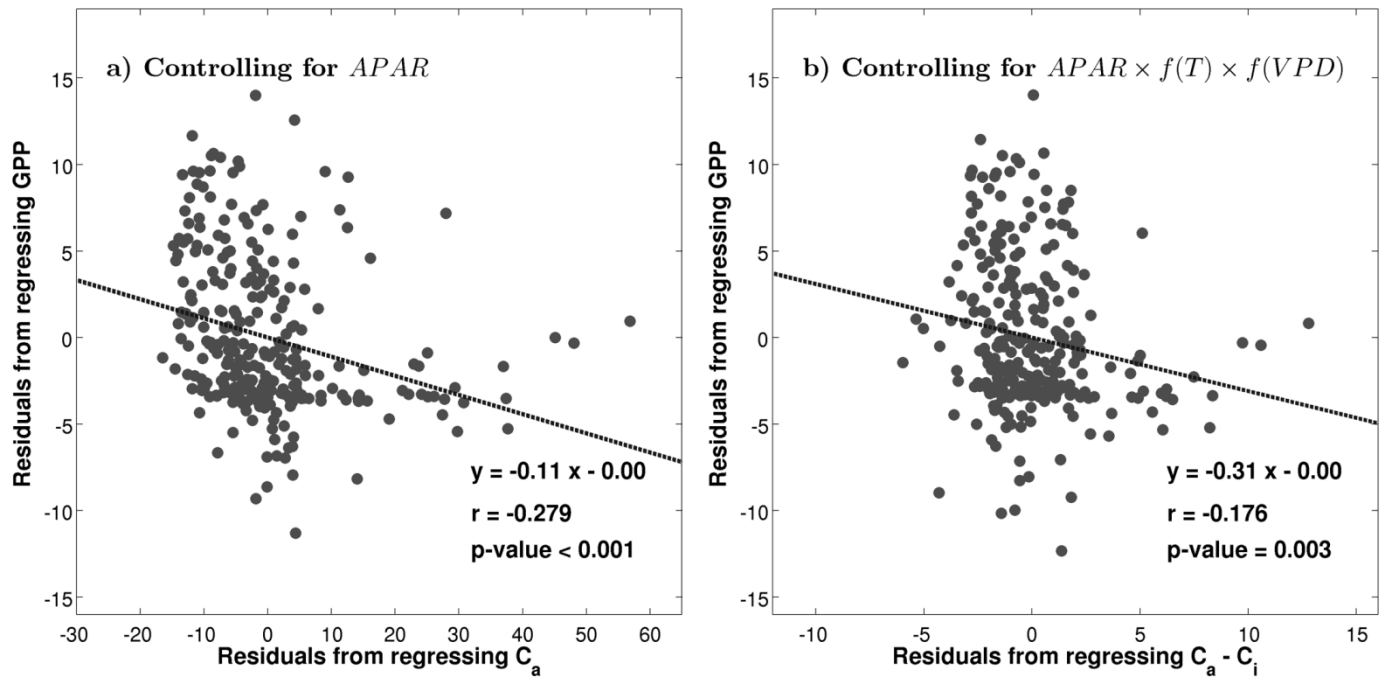
Figure 13: Residual plots are shown for a) the partial correction between GPP and ambient CO_2 concentration (C_a) while controlling for the variable of *APAR* and b) the partial correction between GPP and C_a - C_i while controlling for the variable of $APAR \times f(T) \times f(VPD)$.

5.2 Clumping effects in the GORT model

The clumping effects of leaves modeled using GORT influence canopy radiative transfer processes and are worthy of further examination. Chen et al. (1997) demonstrated that the net effects of leaf clumping could be modeled by introducing a clumping index. We derive the clumping index by inverting their functions (Zhao et al., 2011) as follows:

$$\Omega = \ln(P_{\text{gap}}) / \ln(P_{\text{Beer}}) = -\ln(P_{\text{gap}}) / k_b LAI \tag{58}$$

555 where Ω is the clumping index, P_{gap} is the gap probability modeled using GORT, $P_{\text{Beer}} = \exp(-k_b LAI)$ is

556 the gap probability modeled using Beer's Law, k_b is the extinction coefficient, and *LAI* is the leaf area

557 index.

558

559 The behavior of the derived clumping index shown in Figure 14 is intuitively interpretable. Leaves are more

560 clumped when LAI is larger given constant tree structures. However, when LAI is constant but tree density

561 increases, leaves are distributed in a larger three-dimensional space, resulting in an increased clumping

562 index. Similarly, if the H/b ratio or b/R ratio decreases while other parameters are unchanged, the total

563 crown volume increases and leaves are less clumped. The sensitivity of the clumping index to the

564 illumination zenith angle varies when using different parameter sets. Our simulated results are in line with

565 the measured and modeled results in previous studies (Leblanc and Chen, 2001; Leblanc et al., 2002): the

566 clumping indexes are insensitive to zenith angles in some forest stands and increase with zenith angles in

567 others. We do not attempt to derive clumping indexes at solar zenith angle greater than 85° when gap

568 fractions typically approach zeros. These results imply that tree structure strongly influences radiation

569 absorption and photosynthesis of canopies.

570

571
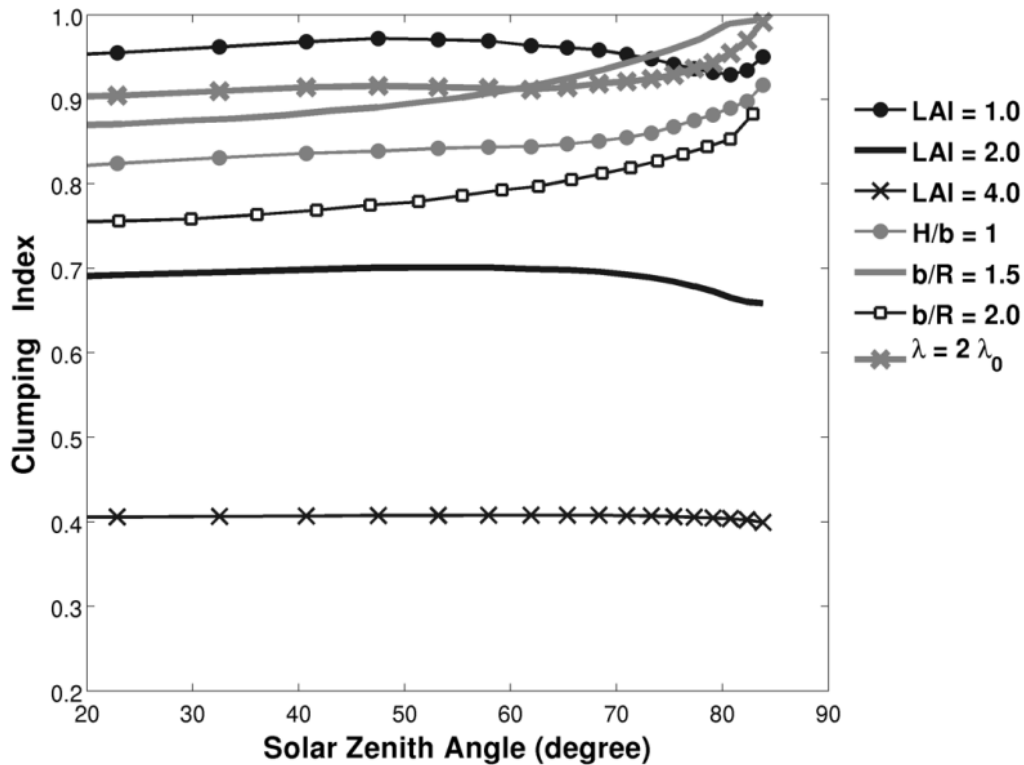
Figure 14: Derived clumping index as a function of solar zenith angle for varied canopy parameters. Tree parameters for US-Bar are used for GORT simulations. The default simulation is for a canopy composed of $H/b = 2.0$, $b/R = 3.0$, $\lambda = 1432$ trees/ha, and $LAI = 2.0$, and labeled curves are for the same case with only the labeled parameters varied.

5.3 Assumptions and future improvements

It is also necessary to review our model assumptions and identify possible avenues for future improvements. First, we assume a spherical leaf angle distribution in the model simulations. However, most deciduous forests have semi-horizontal leaf orientation (Bonan, 2002) and an assumption of planophile or plagiophile LAD is likely to be more appropriate for temperate and boreal broadleaf forests (Pisek et al., 2013). Because LAD influences the proportions of sunlit and shaded leaf areas, the way in which modeled canopy GPP varies with LAD requires further exploration. Second, the substrate under the canopy layer is assumed to be a Lambertian surface. Field studies have observed the effects of bi-directional reflectance distribution function (BRDF) for soils (Liang and Townshend, 1996; Wang et al., 2010), and coupled soil and vegetation model (Ni and Li, 2000; Verhoef and Bach, 2007) should be tested to understand the effects of soil BRDF on canopy photosynthesis. Third, we assume maximum constant leaf stomatal conductance over the

38

growing season. It is worth examining how optimal leaf stomatal conductance may evolve with leaf

development stages and long-term environmental changes (Keenan et al., 2013; Lammertsma et al., 2011).

Fourth, we use ellipsoids to describe tree crown shapes for deciduous broadleaf forests. Because many

evergreen needleleaf forests have conical crowns, future applications to areas with conifer forests may

require different treatment on crown shapes in the models. Finally, our linkage between radiative transfer

and biochemical processes is still empirical. We may need to test other mechanisms, for example, the

biochemical model based on the enzyme kinetics of rubisco and the regeneration of RuBP in response to

light absorption (Farquhar and Sharkey, 1982), in future studies.

6. Conclusion

We propose and validate a new model that links GORT with biochemical processes for modeling canopy

photosynthesis. Several main conclusions can be drawn from this study. First, the radiative transfer process

within the canopy is one of the key factors in modeling vegetation photosynthesis, and our proposed model

simulates canopy photosynthesis well. Modeled GPP robustly explained approximately 80% or more

variance in GPP measurements at both half-hourly and daily time scales. Second, tree structures influence

canopy gap probabilities and vegetation photosynthesis. Leaf clumping could vary as a function of tree

density, canopy depth, and crown shapes and affect canopy sunlight interception. Finally, ambient CO_2

concentrations influence vegetation photosynthesis activities and should be included in biogeochemical

models.

Accurate modeling of vegetation photosynthesis is essential for improving our understanding of the global

carbon cycle. The model we developed is complementary to classic radiative transfer models, especially in

sparse and intermediate forest stands. Although more validation efforts are required, the GORT-

photosynthesis model is promising in terms of simulating photosynthesis for discontinuous plant canopies.

Appendix A:

Table A1. Nomenclature

Symbols	Definition
$P_{\text{gap}}(h, \theta_i)$	total gap probability for beam light passing through the canopy
$P_{\text{gap}}(n = 0 \vert h, \theta_i)$	gap probability for beam light passing through the canopy without reaching any crowns
$P_{\text{gap}}(n > 0 \vert h, \theta_i)$	gap probability for beam light passing through crowns without being intercepted by leaves
$P(s \vert h, \theta_i)$	probability distribution function associated with within-crown path length
$P(s \vert n, z, h, \theta_i)$	probability distribution of within-crown path length given that a solar ray enters the crown at height h and angle θ_i
$P(n \vert z, h, \theta_i)$	probability distribution of the numbers of crowns intercepted by the solar ray incident at angle θ_i, entering crowns at height z, and then traveling to height h
λ_v	tree density (m^{-2})
V_Γ	projected cylinder volume starting from the canopy top and extending to certain height
$\tau(\theta_i, \alpha)$	projected foliage area volume density (m^{-1})
$k_b(\theta_i, \alpha)$	extinction coefficient for beam radiation
k_d	extinction coefficient for diffuse radiation
$K_{\text{open}}(h)$	canopy openness factor to diffuse radiation
$K_{\text{open}}(n = 0 \vert h)$	between-crown openness factor
$K_{\text{open}}(n > 0 \vert h)$	within-crown openness factor
$P'_{\text{gap}}(h, \theta_i)$	the first derivative of gap probability $P_{\text{gap}}(h, \theta_i)$ with respect to height
$K'_{\text{open}}(h)$	the first derivative of the openness factor $K_{\text{open}}(h)$ with respect to height
$t_0(h, \theta_i)$	the proportion of unintercepted direct beam for semi-infinite homogeneous canopies
R_{ff}^∞	hemispherical-hemispherical reflectance for semi-infinite homogeneous canopies
R_{df}^∞	directional-hemispherical reflectance for semi-infinite homogeneous canopies
T_{ff}^∞	hemispherical-hemispherical transmittance for semi-infinite homogeneous canopies
T_{df}^∞	directional-hemispherical transmittance for semi-infinite homogeneous canopies
$\rho_{ff}(h)$	hemispherical-hemispherical reflectance for homogeneous canopies with finite thickness
$\rho_{df}(h, \theta_i)$	directional-hemispherical reflectance for homogeneous canopies with finite thickness
$t_{ff}(h)$	hemispherical-hemispherical transmittance for homogeneous canopies with finite thickness
$t_{df}(h, \theta_i)$	directional-hemispherical transmittance for homogeneous canopies with finite thickness
$\rho'_{ff}(h)$	hemispherical-hemispherical reflectance for discontinuous canopies
$\rho'_{df}(h, \theta_i)$	directional-hemispherical reflectance for discontinuous canopies
$t'_{ff}(h)$	hemispherical-hemispherical transmittance for discontinuous canopies
$t'_{df}(h, \theta_i)$	directional-hemispherical transmittance for discontinuous canopies
$\delta LAI(h)$	leaf area index within a thin layer δh at height h
LAI	total leaf area index of the canopy
$LAI_{Sun}(\theta_i)$	sunlit leaf area index given a solar illumination angle θ_i
$LAI_{Shd}(\theta_i)$	shaded leaf area index given a solar illumination angle θ_i
$LAI_{Sun}^*(\theta_i)$	sunlit leaf area for homogeneous canopies given a solar illumination angle θ_i
θ_i	solar illumination angle
ϕ	azimuth angle
σ	leaf single scattering albedo
γ	$\sqrt{1 - \sigma}$
μ_i	$\cos(\theta_i)$
ρ_l	leaf reflectance
τ_l	leaf transmittance
ρ_s	soil reflectance
ρ_{cb}	canopy reflection coefficient for beam irradiance
ρ_{cd}	canopy reflection coefficient for diffuse irradiance

f_b	the fraction of incident beam radiation in total or global incoming solar radiation
$I_b(h, \theta_i)$	unintercepted beam fluxes at canopy height h given a solar illumination angle θ_i
$I_d(h)$	unintercepted diffuse fluxes at canopy height h
$I_{bt}(h, \theta_i)$	unintercepted and down scattered beam fluxes
$I_{dt}(h)$	unintercepted and down scattered diffuse fluxes
I_c	total radiation absorbed by canopy elements
I_{cb}	beam radiation absorbed by canopy elements
I_{cd}	diffuse radiation absorbed by canopy elements
I_{Sun}	total radiation absorbed by sunlit leaves
I_{Sunb}	beam radiation directly absorbed by sunlit leaves
I_{Sunbs}	down scattered beam radiation absorbed by sunlit leaves
I_{Sund}	diffuse radiation absorbed by sunlit leaves
I_{Sun}	total radiation absorbed by shaded leaves
Q_{Sun}	total radiation absorbed by sunlit leaves per leaf hemi-surface area
Q_{Shd}	total radiation absorbed by shaded leaves per leaf hemi-surface area
A	leaf-level CO_2 assimilation rate
g_c	stomatal conductance
C_a	ambient CO_2 concentrations
C_i	intercellular CO_2 concentrations
g_{cSun}	stomatal conductance for sunlit leaves
g_{cShd}	stomatal conductance for shaded leaves
g_{cmax}	maximum leaf stomatal conductance when environmental factors do not limit carbon uptake
$f(x_i)$	scalars that account for the influences of environmental stresses on leaf stomatal conductance
$f(Q)$	scalars that account for the influences of solar radiation on leaf stomatal conductance
$f(T)$	scalars that account for the influences of temperature on leaf stomatal conductance
$f(VPD)$	scalars that account for the influences of vapor pressure deficit on leaf stomatal conductance
k_C	stress coefficients of PAR absorbed by plant leaves for the temperature scalar
k_Q	stress coefficients of PAR absorbed by plant leaves for the temperature scalar
T_{min}	minimum temperature for photosynthetic activities
T_{max}	maximum temperature for photosynthetic activities
T_{opt}	optimum temperature for photosynthetic activities
VPD	ambient vapor pressure deficit
VPD_{min}	minimum vapor pressure deficit
VPD_{max}	maximum vapor pressure deficit
VPD_0	an empirical constant describing the species sensitivity to ambient vapor pressure deficit
Γ	leaf CO_2 compensation point
m_L	regression coefficient for ambient and intercellular CO_2 concentrations related to tree species
A_{Sun}	leaf-level CO_2 assimilation rate for sunlit leaves
A_{Shd}	leaf-level CO_2 assimilation rate for shaded leaves
K_t	hourly clearness index
I_0	total or global incoming solar radiation on a horizontal plane at the canopy top
I_e	extraterrestrial solar radiation
Ω	foliage clumping index
P_{Beer}	gap probability for beam light passing through the canopy as modeled using Beer's Law

615

616 Table A2. Values for model parameters

Symbols	Value	Units	Reference
k_C	500	W / m²	Ding et al. (2014)
k_Q	150	W / m²	Ding et al. (2014)
T_{min}	0	℃	Kalfas et al. (2011)
T_{max}	45	℃	Kalfas et al. (2011)

T_{opt}	25	℃	Kalfas et al. (2011)
VPD_{min}	0.65	kPa	Heinsch et al. (2003)
VPD_{max}	4.6	kPa	Heinsch et al. (2003)
VPD_0	30	kPa	Katul et al. (2000)
Γ	40	μmol/mol	Katul et al. (2000)
m_L	4.0		Katul et al. (2000)

617

Author contribution

619 Qinchuan Xin developed the model code and performed the simulations. Qinchuan Xin designed the

620 experiments and Wenyu Li contributed to data analysis. Qinchuan Xin and Peng Gong prepared the

621 manuscript with contributions from all co-authors.

622

629

References

631 Allen, R. G., Pereira, L. S., Raes, D., and Smith, M.: Crop evapotranspiration-Guidelines for computing
632 crop water requirements-FAO Irrigation and drainage paper 56, FAO, Rome, 300, 6541, 1998.

633 Baldocchi, D., Falge, E., Gu, L., Olson, R., Hollinger, D., Running, S., Anthoni, P., Bernhofer, C., Davis, K.,
634 and Evans, R.: FLUXNET: A new tool to study the temporal and spatial variability of ecosystem-scale
635 carbon dioxide, water vapor, and energy flux densities, Bulletin of the American Meteorological Society, 82,
636 2415-2434, 2001.

637 Baldocchi, D., Hutchison, B., Matt, D., and McMillen, R.: Canopy radiative transfer models for spherical
638 and known leaf inclination angle distributions: a test in an oak-hickory forest, Journal of Applied Ecology,
639 1985. 539-555, 1985.

640 Baldocchi, D. D.: Assessing the eddy covariance technique for evaluating carbon dioxide exchange rates of
641 ecosystems: past, present and future, Global Change Biology, 9, 479-492, 2003.

642 Ball, J. T., Woodrow, I., and Berry, J.: A Model Predicting Stomatal Conductance and its Contribution to the
643 Control of Photosynthesis under Different Environmental Conditions. In: Progress in Photosynthesis
644 Research, Biggins, J. (Ed.), Springer Netherlands, 1987.

645 Bonan, G. B.: Ecological climatology: concepts and applications, Cambridge University Press, 2002.

646 Bonan, G. B.: Forests and climate change: forcings, feedbacks, and the climate benefits of forests, science,
647 320, 1444-1449, 2008.

648 Broich, M., Huete, A., Tulbure, M. G., Ma, X., Xin, Q., Paget, M., Restrepo-Coupe, N., Davies, K.,
649 Devadas, R., and Held, A.: Land surface phenological response to decadal climate variability across
650 Australia using satellite remote sensing, Biogeosciences, 11, 5181-5198, 2014.

651 Campbell, G. S. and Norman, J. M.: An introduction to environmental biophysics, Springer, 1998.

652 Chen, J. M., Rich, P. M., Gower, S. T., Norman, J. M., and Plummer, S.: Leaf area index of boreal forests:
653 Theory, techniques, and measurements, Journal of Geophysical Research: Atmospheres (1984–2012), 102,
654 29429-29443, 1997.

655 Chen, T., van der Werf, G. R., Dolman, A. J., and Groenendijk, M.: Evaluation of cropland maximum light
656 use efficiency using eddy flux measurements in North America and Europe, Geophysical Research Letters,
657 38, 2011.

658 Collatz, G. J., Ball, J. T., Grivet, C., and Berry, J. A.: Physiological and environmental regulation of stomatal
659 conductance, photosynthesis and transpiration: a model that includes a laminar boundary layer, Agricultural
660 and Forest Meteorology, 54, 107-136, 1991.

661 Cramer, W., Bondeau, A., Woodward, F. I., Prentice, I. C., Betts, R. A., Brovkin, V., Cox, P. M., Fisher, V.,
662 Foley, J. A., and Friend, A. D.: Global response of terrestrial ecosystem structure and function to CO2 and
663 climate change: results from six dynamic global vegetation models, Global change biology, 7, 357-373,
664 2001.

665 Ding, R., Kang, S., Du, T., Hao, X., and Zhang, Y.: Scaling Up Stomatal Conductance from Leaf to Canopy
666 Using a Dual-Leaf Model for Estimating Crop Evapotranspiration, PloS one, 9, e95584, 2014.

667 Fan, W., Chen, J. M., Ju, W., and Nesbitt, N.: Hybrid Geometric Optical Radiative Transfer Model Suitable
668 for Forests on Slopes, IEEE Transactions on Geoscience and Remote Sensing, 52, 5579-5586, 2014.

669 Farquhar, G. D. and Sharkey, T. D.: Stomatal conductance and photosynthesis, Annual review of plant
670 physiology, 33, 317-345, 1982.

671 Field, C. B., Randerson, J. T., and Malmstrom, C. M.: Global net primary production: Combining ecology
672 and remote sensing, Remote Sensing of Environment, 51, 74-88, 1995.

673 Goudriaan, J.: Crop micrometeorology: a simulation study, Pudoc, Center for Agricultural Publishing and
674 Documentation, 1977.

675 Hapke, B.: Bidirectional reflectance spectroscopy: 1. Theory, Journal of Geophysical Research: Solid Earth
676 (1978–2012), 86, 3039-3054, 1981.

677 He, L., Chen, J. M., Pisek, J., Schaaf, C. B., and Strahler, A. H.: Global clumping index map derived from
678 the MODIS BRDF product, Remote Sensing of Environment, 119, 118-130, 2012.

679 He, M., Ju, W., Zhou, Y., Chen, J., He, H., Wang, S., Wang, H., Guan, D., Yan, J., and Li, Y.: Development
680 of a two-leaf light use efficiency model for improving the calculation of terrestrial gross primary
681 productivity, Agricultural and Forest Meteorology, 173, 28-39, 2013.

682 Heimann, M. and Reichstein, M.: Terrestrial ecosystem carbon dynamics and climate feedbacks, Nature,
683 451, 289-292, 2008.

684 Heinsch, F. A., Reeves, M., Votava, P., Kang, S., Milesi, C., Zhao, M., Glassy, J., Jolly, W. M., Loehman, R.,
685 and Bowker, C. F.: GPP and NPP (MOD17A2/A3) Products NASA MODIS Land Algorithm, MOD17
686 User's Guide, 2003. 1-57, 2003.

687 Jarvis, P. G. and McNaughton, K.: Stomatal control of transpiration: scaling up from leaf to region,
688 Advances in ecological research, 15, 1-49, 1986.

689 Kalfas, J. L., Xiao, X., Vanegas, D. X., Verma, S. B., and Suyker, A. E.: Modeling gross primary production
690 of irrigated and rain-fed maize using MODIS imagery and CO_2 flux tower data, Agricultural and Forest
691 Meteorology, 151, 1514-1528, 2011.

692 Katul, G., Ellsworth, D., and Lai, C. T.: Modelling assimilation and intercellular CO_2 from measured
693 conductance: a synthesis of approaches, Plant, Cell & Environment, 23, 1313-1328, 2000.

694 Keenan, T. F., Hollinger, D. Y., Bohrer, G., Dragoni, D., Munger, J. W., Schmid, H. P., and Richardson, A.
695 D.: Increase in forest water-use efficiency as atmospheric carbon dioxide concentrations rise, Nature, 499,
696 324-327, 2013.

697 Kucharik, C. J., Barford, C. C., El Maayar, M., Wofsy, S. C., Monson, R. K., and Baldocchi, D. D.: A
698 multiyear evaluation of a Dynamic Global Vegetation Model at three AmeriFlux forest sites: Vegetation
699 structure, phenology, soil temperature, and CO2 and H2O vapor exchange, Ecological Modelling, 196, 1-31,
700 2006.

701 Lammertsma, E. I., de Boer, H. J., Dekker, S. C., Dilcher, D. L., Lotter, A. F., and Wagner-Cremer, F.:
702 Global CO2 rise leads to reduced maximum stomatal conductance in Florida vegetation, Proceedings of the
703 National Academy of Sciences, 108, 4035-4040, 2011.

704 Law, B., Falge, E., Gu, L. v., Baldocchi, D., Bakwin, P., Berbigier, P., Davis, K., Dolman, A., Falk, M., and
705 Fuentes, J.: Environmental controls over carbon dioxide and water vapor exchange of terrestrial vegetation,
706 Agricultural and Forest Meteorology, 113, 97-120, 2002.

707 Leblanc, S. G. and Chen, J. M.: A practical scheme for correcting multiple scattering effects on optical LAI
708 measurements, Agricultural and Forest Meteorology, 110, 125-139, 2001.

709 Leblanc, S. G., Chen, J. M., and Kwong, M.: Tracing radiation and architecture of canopies, TRAC Manual.
710 Version, 2, 25, 2002.

711 Leuning, R.: A critical appraisal of a combined stomatal‐photosynthesis model for C3 plants, Plant, Cell &
712 Environment, 18, 339-355, 1995.

713 Li, L., Friedl, M. A., Xin, Q., Gray, J., Pan, Y., and Frolking, S.: Mapping Crop Cycles in China Using
714 MODIS-EVI Time Series, Remote Sensing, 6, 2473-2493, 2014.

715 Li, X. and Strahler, A. H.: Geometric-optical bidirectional reflectance modeling of the discrete crown
716 vegetation canopy: Effect of crown shape and mutual shadowing, IEEE Transactions on Geoscience and
717 Remote Sensing, 30, 276-292, 1992.

718 Li, X., Strahler, A. H., and Woodcock, C. E.: A hybrid geometric optical-radiative transfer approach for
719 modeling albedo and directional reflectance of discontinuous canopies, IEEE Transactions on Geoscience
720 and Remote Sensing, 33, 466-480, 1995.

721 Liang, S. and Townshend, J.: A parametric soil BRDF model: A four stream approximation for multiple
722 scattering, International journal of remote sensing, 17, 1303-1315, 1996.

723 Liu, J., Woodcock, C. E., Melloh, R. A., Davis, R. E., McKenzie, C., and Painter, T. H.: Modeling the view
724 angle dependence of gap fractions in forest canopies: Implications for mapping fractional snow cover using
725 optical remote sensing, Journal of Hydrometeorology, 9, 1005-1019, 2008.

726 Monteith, J. L.: Climate and efficiency of crop production in Britain, Philosophical Transactions of the
727 Royal Society of London Series B-Biological Sciences, 281, 277-294, 1977.

728 Muneer, T.: Solar radiation and daylight models, Routledge, 2007.

729 Myneni, R., Maggion, S., Iaquinta, J., Privette, J., Gobron, N., Pinty, B., Kimes, D., Verstraete, M., and
730 Williams, D.: Optical remote sensing of vegetation: modeling, caveats, and algorithms, Remote Sensing of
731 Environment, 51, 169-188, 1995.

732 Myneni, R. B.: Modeling radiative transfer and photosynthesis in three-dimensional vegetation canopies,
733 Agricultural and Forest Meteorology, 55, 323-344, 1991.

734 Myneni, R. B., Asrar, G., and Gerstl, S. A.: Radiative transfer in three dimensional leaf canopies, Transport
735 Theory and Statistical Physics, 19, 205-250, 1990.

736 Myneni, R. B., Hoffman, S., Knyazikhin, Y., Privette, J. L., Glassy, J., Tian, Y., Wang, Y., Song, X., Zhang,
737 Y., Smith, G. R., Lotsch, A., Friedl, M., Morisette, J. T., Votava, P., Nemani, R. R., and Running, S. W.:
738 Global products of vegetation leaf area and fraction absorbed PAR from year one of MODIS data, Remote
739 Sensing of Environment, 83, 214-231, 2002.

740 Myneni, R. B., Keeling, C., Tucker, C., Asrar, G., and Nemani, R.: Increased plant growth in the northern
741 high latitudes from 1981 to 1991, Nature, 386, 698-702, 1997.

742 Ni-Meister, W., Yang, W., and Kiang, N. Y.: A clumped-foliage canopy radiative transfer model for a global
743 dynamic terrestrial ecosystem model. I: Theory, Agricultural and forest meteorology, 150, 881-894, 2010.

744 Ni, W.: Development and application of models of the radiation regime within conifer forests, 1998.

745 Ni, W. and Li, X.: A coupled vegetation–soil bidirectional reflectance model for a semiarid landscape,
746 Remote Sensing of Environment, 74, 113-124, 2000.

747 Ni, W., Li, X., Woodcock, C. E., Caetano, M. R., and Strahler, A. H.: An analytical hybrid GORT model for
748 bidirectional reflectance over discontinuous plant canopies, IEEE Transactions on Geoscience and Remote
749 Sensing, 37, 987-999, 1999.

750 Ni, W., Li, X., Woodcock, C. E., Roujean, J. L., and Davis, R. E.: Transmission of solar radiation in boreal
751 conifer forests: Measurements and models, Journal of Geophysical Research: Atmospheres (1984–2012),
752 102, 29555-29566, 1997.

753 Pearcy, R. W., Schulze, E.-D., and Zimmermann, R.: Measurement of transpiration and leaf conductance. In:
754 Plant physiological ecology, Springer, 1989.

Pearcy, R. W. and Sims, D. A.: Photosynthetic acclimation to changing light environments: scaling from the leaf to the whole plant, Exploitation of environmental heterogeneity by plants, 1994. 145-174, 1994.

Peng, S., Piao, S., Zeng, Z., Ciais, P., Zhou, L., Li, L. Z., Myneni, R. B., Yin, Y., and Zeng, H.: Afforestation in China cools local land surface temperature, Proceedings of the National Academy of Sciences, 111, 2915-2919, 2014.

Pisek, J., Sonnentag, O., Richardson, A. D., and Mõttus, M.: Is the spherical leaf inclination angle distribution a valid assumption for temperate and boreal broadleaf tree species?, Agricultural and Forest Meteorology, 169, 186-194, 2013.

Potter, C. S., Randerson, J. T., Field, C. B., Matson, P. A., Vitousek, P. M., Mooney, H. A., and Klooster, S. A.: Terrestrial ecosystem production - a process model-based on global satellite and surface data, Global Biogeochemical Cycles, 7, 811-841, 1993.

Prince, S. D. and Goward, S. N.: Global primary production: A remote sensing approach, Journal of Biogeography, 22, 815-835, 1995.

Pury, D. d. and Farquhar, G.: Simple scaling of photosynthesis from leaves to canopies without the errors of big‐leaf models, Plant, Cell & Environment, 20, 537-557, 1997.

Raich, J., Rastetter, E., Melillo, J., Kicklighter, D., Steudler, P., Peterson, B., Grace, A., Moore Iii, B., and Vörösmarty, C.: Potential net primary productivity in South America: application of a global model, Ecological Applications, 1991. 399-429, 1991.

Richardson, A. D., Anderson, R. S., Arain, M. A., Barr, A. G., Bohrer, G., Chen, G. S., Chen, J. M., Ciais, P., Davis, K. J., Desai, A. R., Dietze, M. C., Dragoni, D., Garrity, S. R., Gough, C. M., Grant, R., Hollinger, D. Y., Margolis, H. A., McCaughey, H., Migliavacca, M., Monson, R. K., Munger, J. W., Poulter, B., Raczka, B. M., Ricciuto, D. M., Sahoo, A. K., Schaefer, K., Tian, H. Q., Vargas, R., Verbeeck, H., Xiao, J. F., and Xue, Y. K.: Terrestrial biosphere models need better representation of vegetation phenology: results from the North American Carbon Program Site Synthesis, Global Change Biology, 18, 566-584, 2012.

Running, S. W., Nemani, R. R., Heinsch, F. A., Zhao, M. S., Reeves, M., and Hashimoto, H.: A continuous satellite-derived measure of global terrestrial primary production, Bioscience, 54, 547-560, 2004.

Running, S. W., Thornton, P. E., Nemani, R., and Glassy, J. M.: Global terrestrial gross and net primary productivity from the earth observing system, Methods in Ecosystem Science, 2000. 44-57, 2000.

Ryu, Y., Baldocchi, D. D., Kobayashi, H., Ingen, C., Li, J., Black, T. A., Beringer, J., Gorsel, E., Knohl, A., and Law, B. E.: Integration of MODIS land and atmosphere products with a coupled‐process model to estimate gross primary productivity and evapotranspiration from 1 km to global scales, Global Biogeochemical Cycles, 25, GB4017, 2011.

787   Schaaf, C. B., Li, X., and Strahler, A.: Topographic effects on bidirectional and hemispherical reflectances
788   calculated with a geometric-optical canopy model, IEEE Transactions on Geoscience and Remote Sensing,
789   32, 1186-1193, 1994.

790   Schulze, E.-D., Kelliher, F. M., Korner, C., Lloyd, J., and Leuning, R.: Relationships among maximum
791   stomatal conductance, ecosystem surface conductance, carbon assimilation rate, and plant nitrogen nutrition:
792   a global ecology scaling exercise, Annual Review of Ecology and Systematics, 1994. 629-660, 1994.

793   Sellers, P. J.: Canopy reflectance, photosynthesis and transpiration, International Journal of Remote Sensing,
794   6, 1335-1372, 1985.

795   Sjöström, M., Zhao, M., Archibald, S., Arneth, A., Cappelaere, B., Falk, U., De Grandcourt, A., Hanan, N.,
796   Kergoat, L., and Kutsch, W.: Evaluation of MODIS gross primary productivity for Africa using eddy
797   covariance data, Remote Sensing of Environment, 131, 275-286, 2013.

798   Song, C., Katul, G., Oren, R., Band, L. E., Tague, C. L., Stoy, P. C., and McCarthy, H. R.: Energy, water,
799   and carbon fluxes in a loblolly pine stand: Results from uniform and gappy canopy models with
800   comparisons to eddy flux data, Journal of Geophysical Research: Biogeosciences, 114, G04021, 2009.

801   Strahler, A. H., Muller, J., Lucht, W., Schaaf, C., Tsang, T., Gao, F., Li, X., Lewis, P., and Barnsley, M. J.:
802   MODIS BRDF/albedo product: algorithm theoretical basis document version 5.0, MODIS documentation,
803   1999. 1999.

804   Verhoef, W. and Bach, H.: Coupled soil–leaf-canopy and atmosphere radiative transfer modeling to simulate
805   hyperspectral multi-angular surface reflectance and TOA radiance data, Remote Sensing of Environment,
806   109, 166-182, 2007.

807   Wang, Z., Coburn, C., Ren, X., Mazumdar, D., Myshak, S., Mullin, A., and Teillet, P.: Assessment of soil
808   surface BRDF using an imaging spectrometer, 2010, 783010-783019.

809   Xia, J., Chen, J., Piao, S., Ciais, P., Luo, Y., and Wan, S.: Terrestrial carbon cycle affected by non-uniform
810   climate warming, Nature Geoscience, 2014. 2014.

811   Xin, Q., Broich, M., Suyker, A. E., Yu, L., and Gong, P.: Multi-scale evaluation of light use efficiency in
812   MODIS gross primary productivity for croplands in the Midwestern United States, Agricultural and Forest
813   Meteorology, 201, 111-119, 2015.

814   Xin, Q., Gong, P., Yu, C., Yu, L., Broich, M., Suyker, A. E., and Myneni, R. B.: A Production Efficiency
815   Model-Based Method for Satellite Estimates of Corn and Soybean Yields in the Midwestern US, Remote
816   Sensing, 5, 5926-5943, 2013.

817 Xin, Q., Woodcock, C. E., Liu, J., Tan, B., Melloh, R. A., and Davis, R. E.: View angle effects on MODIS
818 snow mapping in forests, Remote Sensing of Environment, 118, 50-59, 2012.

819 Xu, L., Myneni, R., Chapin III, F., Callaghan, T., Pinzon, J., Tucker, C., Zhu, Z., Bi, J., Ciais, P., and
820 Tømmervik, H.: Diminished temperature and vegetation seasonality over northern high latitudes, Nature
821 Climate Change, 2013. 2013.

822 Yang, W., Ni-Meister, W., Kiang, N. Y., Moorcroft, P. R., Strahler, A. H., and Oliphant, A.: A clumped-
823 foliage canopy radiative transfer model for a Global Dynamic Terrestrial Ecosystem Model II: Comparison
824 to measurements, Agricultural and Forest Meteorology, 150, 895-907, 2010.

825 Yang, X., Strahler, A. H., Schaaf, C. B., Jupp, D. L., Yao, T., Zhao, F., Wang, Z., Culvenor, D. S., Newnham,
826 G. J., and Lovell, J. L.: Three-dimensional forest reconstruction and structural parameter retrievals using a
827 terrestrial full-waveform lidar instrument (Echidna®), Remote sensing of environment, 135, 36-51, 2013.

828 Yao, T., Yang, X., Zhao, F., Wang, Z., Zhang, Q., Jupp, D., Lovell, J., Culvenor, D., Newnham, G., and Ni-
829 Meister, W.: Measuring forest structure and biomass in New England forest stands using Echidna ground-
830 based lidar, Remote sensing of Environment, 115, 2965-2974, 2011.

831 Yi, C., Ricciuto, D., Li, R., Wolbeck, J., Xu, X., Nilsson, M., Aires, L., Albertson, J. D., Ammann, C., and
832 Arain, M. A.: Climate control of terrestrial carbon exchange across biomes and continents, Environ. Res.
833 Lett., 5, 034007, 2010.

834 Yuan, H., Dickinson, R. E., Dai, Y., Shaikh, M. J., Zhou, L., Shangguan, W., and Ji, D.: A 3D Canopy
835 Radiative Transfer Model for Global Climate Modeling: Description, Validation, and Application, Journal of
836 Climate, 27, 1168-1192, 2013.

837 Zhang, Q., Cheng, Y., Lyapustin, A. I., Wang, Y., Xiao, X., Suyker, A., Verma, S., Tan, B., and Middleton, E.
838 M.: Estimation of crop gross primary production (GPP): I. impact of MODIS observation footprint and
839 impact of vegetation BRDF characteristics, Agricultural and Forest Meteorology, 191, 51-63, 2014.

840 Zhang, Q., Xiao, X., Braswell, B., Linder, E., Baret, F., and Moore Iii, B.: Estimating light absorption by
841 chlorophyll, leaf and canopy in a deciduous broadleaf forest using MODIS data and a radiative transfer
842 model, Remote Sensing of Environment, 99, 357-371, 2005.

843 Zhang, X., Friedl, M. A., Schaaf, C. B., Strahler, A. H., Hodges, J. C., Gao, F., Reed, B. C., and Huete, A.:
844 Monitoring vegetation phenology using MODIS, Remote Sensing of Environment, 84, 471-475, 2003.

845 Zhao, F., Yang, X., Schull, M. A., Román-Colón, M. O., Yao, T., Wang, Z., Zhang, Q., Jupp, D. L., Lovell, J.
846 L., and Culvenor, D. S.: Measuring effective leaf area index, foliage profile, and stand height in New
847 England forest stands using a full-waveform ground-based lidar, Remote Sensing of Environment, 115,
848 2954-2964, 2011.

49

849   Zhao, M., Heinsch, F. A., Nemani, R. R., and Running, S. W.: Improvements of the MODIS terrestrial gross
850   and net primary production global data set, Remote Sensing of Environment, 95, 164-176, 2005.
851
852